TECHNICAL MEMORANDUMS

NATIONAL ADVISORY COMMITTEE FOR AERONAUTICS

No. 1009

THEORETICAL SOLUTION OF PROFILE DRAG

By J. Pretsch

Jahrbuch 1938 der deutschen Luftfahrtforschung

Washington
April 1942

NATIONAL ADVISORY COMMITTEE FOR AERONAUTICS

TECHNICAL MEMORANDUM NO. 1009

THEORETICAL SOLUTION OF PROFILE DRAG*

By J. Pretsch

SUMMARY

After a survey of the customary procedures for appraising the profile drag in which pressure drag was discounted and of the methods for computing the laminar and turbulent friction flow, the author proposes a method by which the pressure drag can be computed with the aid of the displacement thickness of the frictional layer. The method is restricted to the case where the effects, caused by separation of frictional layer, are small. Then the t tal profile drag can be expressed solely by quantities derived from the velocity distribution in the frictional layer immediately at the trailing edge. It is merely assumed thereby that the mixing losses originating over the short length in the wake are negligible until the pressure reaches its end value. The proposed method is applied to seven symmetrical Karman-Trefftz profiles at zero lift and varying position of transitional region. The actual position of the transitional region is deduced by comparison with the measured drag coefficients. Judged by these mathematical results and the available test data the inference is drawn that the position of the transitional region is principally dependent upon the Reynolds number Re_ϑ referred to momentum thickness, but for the rest almost independent of the pressure gradient while being materially affected by the degree of turbulence and surface roughness; the pressure gradient becomes naturally effective in the quantity Re_ϑ itself. This supposition is utilized to predict the transitional region and hence the profile drag coefficient of a smooth wing at moderate degree of turbulence and very large Reynolds numbers ($10^7 < Re < 10^8$) and to compute the friction and pressure drag. It seems as if the percent proportion of the pressure drag to the total profile drag increases with the Reynolds number.

---

*"Zur theoretischen Berechnung des Profilwiderstandes." Reprint from Jahrbuch 1938 der deutsche Luftfahrtforschung, pp. I 60 – I 81.

In conclusion the most urgent problems of the future are enumerated, with the solution of which an improvement in the theoretical profile drag computation may be anticipated.

Notation

Velocities (m/s):

u_∞ flying speed

u_o velocity at the outer boundary of the frictional layer

u tangential component of the velocity within the frictional layer

v normal component of the velocity within the frictional layer

Lengths (m)

x coordinate of a point of the wing in flight direction measured from the stagnation point

y coordinate of a point of the wing in span direction

z coordinate of a point of the wing at right angles to x, y plane

s arc length of a point of the wing measured from stagnation point

n distance from surface of wing

t wing chord

D_{max} maximum profile thickness

b span

δ Pohlhausen's boundary layer thickness

δ^* displacement thickness

ϑ momentum thickness

Angles:

β angle between profile tangent and flight direction

φ trailing edge

Pressure (kg/m^2)

p static pressure

q dynamic pressure

$\zeta = q_\eta$ difference in dynamic pressures at the friction layer boundary and at the point of momentum thickness

τ_o shearing stress

Forces per unit length of span (kg/m)

W force in flight direction

W_p profile drag

W_r frictional drag

W_d pressure drag

Other physical quantities:

ρ air density $\left[\frac{kg\ s^2}{m^4}\right]$

μ air viscosity $\left[\frac{kg\ s}{m^2}\right]$

ν kinematic viscosity $\left[\frac{m^2}{s}\right]$

E yield of a source $\left[\frac{m^3}{s}\right]$

$Z = \frac{\delta^2}{\nu}$ (s)

Dimensionless quantities:

d maximum thickness in ratio to wing chord

f maximum camber in ratio to wing chord

c_a lift coefficient

c_{w_p} coefficient of profile drag

c_{w_r} coefficient of friction drag

c_{w_d} coefficient of pressure drag

$$Re = \frac{u_\infty \, t}{\nu}$$

$$Re_{\delta^*} = \frac{u_o \, \delta^*}{\nu}$$

$$Re_{\vartheta} = \frac{u_o \, \vartheta}{\nu}$$

$$Re^*_{\delta^*} = \frac{u_o^* \, \delta^*}{\nu} \; ; \; u_o^* = \sqrt{\frac{\tau_o}{\rho}}$$

} Reynolds numbers

$$\lambda = \frac{\delta^2}{\nu} \frac{d \, u_o}{d \, s}$$ Pohlhausen's form parameter

$$\eta = 1 - \left[\frac{u(\vartheta)}{u_o} \right]^2$$ Gruschwitz' form parameter

$$H = \frac{\delta^*}{\vartheta}$$

$$\Gamma_1 = - \frac{\delta^*}{u_o} \frac{d \, u_o}{d \, s} \left[\frac{u_o \, \delta^*}{\nu} \right]^{1/4}$$ Nikuradse's form parameter

$$T_1 = \frac{\tau_o}{\rho \, u_o^2} \left[\frac{u_o \, \delta^*}{\nu} \right]^{1/4}$$ dimensionless shearing stress

Indices:

u transitional region of friction layer

a separation point of friction layer

I. INTRODUCTION

Division of Profile Drag in Friction and Pressure Drag

The aim of the present investigation is to compute the profile drag of a wing or of any other cylindrical body with streamlined profile without resorting to measurements. There is no or only insignificant separation of the friction layer on such profile forms at small angles of attack. The profile drag is predominantly skin friction and relatively small in comparison to bodies with considerable spread of separation. The study is confined to such "bodies of low drag," and of these to such with approximately two-dimensional flow.

Since on the modern high-speed aircraft the profile drag can amount to about half of the total drag the problem of theoretical solution is accorded great practical significance. It is rendered difficult by the multiplicity of effects which are able to modify the magnitude of the profile drag.

Whereas the induced drag depends solely on the design of the wing at full scale, that is, its contour and its profile and is computable from the drawing board design itself for all flight cases, the profile drag is also dependent upon the method of construction, such as roughness, waviness in covering, position of rivet head rows, flap gaps, etc., and in flight close to the ground on local weather conditions, that is, the degree of turbulence of the air streaming past the wing.

In order to compute the profile drag the wing must, in the true sense of the word, be put under the magnifying glass, by reason of the fact that the drag is largely induced by the processes taking place in the immediate proximity of the wing surface, namely, in the friction layer.

The air, by adhering to the surface of the wing because of its viscosity, transmits a shearing stress τ_o to it; this stress acts, in two-dimensional flow, in direction of the tangent to the wing profile.

If, starting at the stagnation point, the arc length is denoted with s and the coordinate of a point of the wing in flow direction with x, the resultant W_r of all shearing stresses in flight direction referred to unit length of span b (fig. 1) is:

$$W_r = \int_{I+II} \tau_o \cos \beta \, ds = \int_{I+II} \tau_o \, dx \qquad (1)$$

where β denotes the angle between profile tangent and flight direction and subscripts I and II indicate that the integration from the stagnation point is to be extended once over the suction side and once over the pressure side. The force $W_r b$ is termed the friction drag of the wing; it represents the first portion of the profile drag.

The second loss inducing effect of the air viscosity is the changed pressure distribution along the total wing contour due to the pushing aside of the potential flow. These losses occur even on low drag bodies, but become especially apparent when the friction layer separates, because it no longer possesses sufficient kinetic energy to meet a strong pressure rise of the potential flow. Behind the separation point the pressure actually prevailing does not rise again appreciably; therefore a low-pressure region builds up, and the wing is sucked backward against the direction of flight.

With p denoting the static pressure and z the coordinate of a profile point at right angle to the direction of flight, the resultant W_d of all normally acting forces in flight direction, referred to unit length of span b (fig. 2) is:

$$W_d = \int_{I+II} p \sin \beta \, ds = \int_{I+II} p \, dz \qquad (2)$$

the subscripts I and II having the same meaning as in equation (1). The force $W_d b$ is termed the pressure drag of the wing.

The shearing stress τ_o, through which the frictional drag is computed according to (1) can at least be approximated by the calculation of the friction layer. And, if it succeeds in reducing the pressure drag to quantities that characterize the friction layer, the problem of profile drag reduces to that of defining the friction layer along the wing. This method is to be developed in the present report.

II. PREVIOUS THEOREMS FOR PROFILE DRAG APPRAISAL

Reduction to Profile Drag of Flat Plate

The only body on which the profile drag has been amenable to solution is the thin, flat plate tangentially exposed to a flow of constant speed u_∞. Its pressure drag is zero because all pressures are at right angles to the direction of motion; its profile drag consists therefore exclusively of frictional drag. To compute this frictional drag, three cases must be differentiated theoretically, depending upon the character of flow within the friction layer.

a) The flow within the friction layer past the entire plate is laminar. In this instance the drag coefficient of the plate referred to the base surface is, according to Blasius (reference 1):

$$c_{w_p} = \frac{2.656}{\sqrt{Re}}; \quad Re = \frac{u_\infty t}{\nu} \tag{3}$$

where t is plate length; ν, kinematic viscosity. This law holds true up to about $Re = 5 \times 10^5$.

b) The friction layer along the plate is turbulent. In this case

$$c_{w_p} = \frac{0.91}{(\log_{10} Re)^{2.58}} \tag{4}$$

up to any large values of Re, according to Schlichting (reference 1).

c) The flow is first laminar, then turbulent. The transition from one to the other takes place over a distance of finite length, but may be visualized for the drag calculation as being localized in a point whose distance x from the leading edge can be defined by

$$\frac{u_\infty x}{\nu} \sim 5 \times 10^5 \tag{5}$$

whereby

$$c_{w_p} = \frac{0.91}{(\log_{10} Re)^{2.58}} - \frac{3400}{Re} \tag{6}$$

likewise holds for any Reynolds number, according to Prandtl (reference 2).

The simplifying assumption of sudden reversal signifies that on the transitional distance the actual shearing stress distribution (fig. 3, solid curve) is replaced by the laws for purely laminar or purely turbulent friction layer flow (fig. 3, dotted curve), which has no effect on the integral value of the drag.

The formulas cited refer to the smooth plate; although those for rough plates have also been studied exhaustively by Prandtl and Schlichting (reference 3). Since the profile drag law of the thin, flat plate of the "friction sheet," as we shall call it for short, is known, it is explicable why it has been repeatedly attempted to estimate the profile drag of a wing, even that of an airship hull, by substitution of an "equivalent friction sheet" (Jones, Hoerner, Betz, Bock, Dryden, and Kuethe).

The roughest approximation is obtained with Jones (reference 4) when the wing is replaced by a just-as-fast flying smooth plate of the same depth, the base of which is equal to half the total wing surface.

Hoerner (reference 5) computes the profile drag of modern, high-speed aircraft as friction drag of likewise identically fast but also just-as-rough friction sheets conformal to the Prandtl-Schlichting formulas for rough, flat plates (reference 3).

Hoerner and Jones' approximations make no allowance for the relationship between shearing stress and pressure distribution, which Betz (reference 6) had attempted to estimate back in 1915. For, on assuming that the shearing stress τ_o is proportional to the square of the speed u_o on the outer boundary of the friction layer, the friction drag coefficient of the wing in ratio to that of the equivalent sheet is:

$$\frac{c_{w_r\ \text{wing}}}{c_{w\ \text{plate}}} = \int \left(\frac{u_o}{u_\infty} \right)^2 d\,\frac{s}{t} \qquad (7)$$

where t is wing chord; u_∞, the flying speed.

An estimation of wing friction drag similar to that by Betz is afforded in the proposal by Bock (reference 7), namely, to take the flying speed of the equivalent fric-

tion sheet equal to the "mean flow velocity" past the wing, but fails to give general directions regarding the type of averaging.

Dryden and Kuethe (reference 8) go a step farther in the appraisal of the profile drag of airship hulls, which is mentioned here because their method would be equally applicable to airfoils. The area of the "substitute plate" is computed first, its width at a given distance from the front edge being equal to half the circumference of the airship ring at the same distance from the nose. This "flattened airship" is cut along that "ring" at which the reversal from laminar to turbulent friction layer flow is assumed. On the forebody of the plate the friction layer is laminar, on the afterbody, turbulent. The profile drag of the "stern plate" Dryden and Kuethe compute on the assumption that the flow velocity everywhere is equal to the speed u_∞ of the airship. But the profile drag of the "nose plate" they compute on the assumption that the speed outside of the friction layer changes from one ring to the next exactly as the velocity u_o on the airship. Then a linear theorem for the velocity distribution within the laminar friction layer enables them to compute the shearing stress τ_o and hence the drag of the forward portion of the friction sheet on the basis of Von Karman's momentum equation.

This method of friction sheet analogy is now subjected to a critical analysis:

a) One obvious defect is that the pressure drag cannot be solved at all by theoretical computation. This defect is so much more palpable as the profile is thicker.

But even the friction drag itself cannot be properly determined by this method and for the following reasons:

b) The shearing stress in the laminar as in the turbulent zone of the friction layer is definitely dependent upon the pressure distribution along the profile contour. Dryden and Kuethe allowed for this in the laminar portion, but not in the turbulent.

c) The position of the transitional region depends, according to (5), not only on the Reynolds number Re, but also on the pressure variation and on the degree of turbulence.

d) The angle β between arc element and flight direction is other than zero on the airfoil; hence the shearing stress is effective with only one component, though on slender profiles the error involved is quite small.

However, the discrepancies enumerated of the characteristics of an airfoil from those of an equivalent flat plate may be so pronounced as to make the application of the analogy between the two very restricted.

Statistical Appraisal of Experimental Results

This method consists of evaluating experimentally secured values on a multitude of airfoils statistically so as to afford a practical empirical formula for computing the profile drag for given profile parameters, if possible in respect to angle of attack. In addition to this, a couple of tables from which eventual increments for degree of turbulence, surface condition, etc., could be read off, would be desirable.

One problem found to be very deterrent in this method concerned the extent to which model tests are at all comparable when carried out in different wind tunnels, that is, different turbulence factors, different surface finish, and possibly different wing tip design (references 9, 10).

Moreover, this method will not afford any insight into the mechanism of profile drag, perhaps in connection with friction and pressure drag, in role of the transitional region or the area of separation. Statistical correlation of recorded total drag values will simply lead to statements concerning the total profile drag, unless additional measurements, as, for instance, of the pressure distribution along the profile contour or of the velocity distribution in the friction layer are available for each airfoil.

Munk (reference 11) evidently in continuation of earlier studies (reference 12) gives the following rough rule for the profile drag coefficient

$$c_{w_p} = 0.01 + \frac{d - 0.1}{16} + \frac{f - 0.04}{50} + 0.01\, c_a^3 \qquad (8)$$

where d and f denote thickness and camber in ratio to

wing chord, c_a the lift coefficient. But c_{w_p} is never to be less than 0.006; this minimum value defines the drag of a plate at $Re = 10^6$.

Another formula by Jacobs, Ward, and Pinkerton (reference 13) obtained from measurements on 78 different profiles reads:

$$c_{w_p} = c_{w_{p\ min}} + \Delta c_{w_p} \qquad (9)$$

for symmetrical profiles (subscript s):

$$c_{w_{p\ s\ min}} = 0.0056 + 0.01\ d + 0.1\ d^2 \qquad (10)$$

where d is thickness in ratio to wing chord.

For cambered profiles of the same thickness:

$$c_{w_{p\ min}} = c_{w_{p\ s\ min}} + k;\quad k > 0 \qquad (11)$$

k is shown in the diagrams plotted against position and amount of maximum camber. The angle of attack increment Δc_{w_p} can also be read off from charts.

According to Doetsch and Kramer (reference 10) the measurements in the NACA variable-density tunnel, evaluated in reference (13), yielded, because of the high turbulence factor (critical sphere characteristic $Re_k = 1.2 \times 10^5$) and the blunt wing tips involving an additional pressure drag at the tips, profile drag coefficients by about 18 to 35 percent too high. So the formula (9) should afford at best a qualitatively correct picture.

Very comprehensive is the comparison of profile drag coefficients carried out by Glass (reference 14). He studied the change of minimum profile drag with the Reynolds number but disclaimed the angle of attack relation. The effect due to turbulence he dismisses as negligible on the basis of a report by Hoerner (reference 15). This is obviously due to some misinterpretation. Glass also ultimately reduced the profile drag of a wing to the drag of an equivalent, identically rough friction sheet, just as Hoerner did, but, contrary to Hoerner, he allowed for the effect of profile parameter by a correction factor.

Glass first divided the coefficient of the profile drag into two parts:

$$c_{w_{p\ min}} = c_{w\ plate} + \Delta\ c_{w_p} \tag{12}$$

The first part represents the drag of the equivalent friction sheet with the plan form and surface condition of the wing. The second part is a function of the geometric determinative pieces of the profile which is again split into

$$\Delta\ c_{w_p} = \Delta\ c_{w_r} + c_{w_d} \tag{13}$$

Here $\Delta\ c_{w_r}$ denotes the cumulative friction drag "due to surface curvature," that is, the excess of wing friction drag relative to friction drag of equivalent plate; c_{w_d} is the coefficient of pressure drag.

From the evaluation of extensive test data from German, English, U.S., and Russian wind tunnels, Glass established the following remarkable facts:

a) Independent of Reynolds number and airfoil shape is:

$$\frac{c_{w_d}}{\Delta\ c_{w_r}} \sim \text{const} = 0.85 \tag{14}$$

This law is deduced from tests by Fage, Falkner and Walker (reference 16) on seven symmetrical Karman-Trefftz profiles, in which the pressure distribution was also recorded experimentally. A detailed discussion on this subject follows.

b) Thickness d and camber f, both referred to wing chord, can be combined in a single geometric parameter, the so-called "equivalent thickness" d^*

$$d^* = d + 0.17\ f^2 \tag{15}$$

then it is found that by given Re, the profile drag portion $\Delta\ c_{w_p}$ grows linearly with the equivalent thickness d^*

$$\Delta\ c_{w_p} = K\ (Re)\ d^* \tag{16}$$

Division of the factor K in the product

$$K\,(Re) = n\,(Re)\; c_{w_{plate}}\,(Re) \qquad (17)$$

gives, finally,

$$c_{w_{p\ min}} = c_{w\ plate}\,[1 + n\,(Re)\; d^*] \qquad (18)$$

where $c_{w_{plate}}$ can be computed by the Prandtl-Schlichting formulas, n is represented as explicit function of Re.

Glass quotes $3 \times 10^5 < Re < 9 \times 10^6$ as the range of validity of his empirical formula (18); it is the very zone in which, on the smooth friction sheet, the flow changes from laminar to turbulent. So the initial curve $d^* = 0$ is exactly Prandtl's transition curve (6):

But even Glass' formula, as meritorious as it is, can, because of the discounted effects of turbulence and limitation to minimum drag value, neither make claim to the desired perfection nor, because of the defective comparability of the test values, even to satisfactory accuracy.

In the following it is attempted to compute with the means available the profile drag in theoretical manner, by reducing its two proportions, the pressure and friction drag to quantities that characterize the friction layer. Even though the computation of the friction layer which becomes necessary herewith, and that of the profile drag is in many points still beset with uncertainties, it nevertheless affords a valuable explanation of the question what circumstances are primarily decisive for the drag and so point out the possibilities of lowering the drag.

III. FRICTION LAYERS ON A WING

First we secure a qualitative picture of the flow in the friction layer of a wing. Near the stagnation point the air stream will be laminar. Next follows a transitional region in which the laminar flow turns turbulent, then comes a distance with fully developed turbulence within the friction layer, and, lastly, the potential separation, if the pressure rise is large enough, followed by a dead-air region extending from separation point to trailing edge.

Restricted to bodies of low drag the problem of computing the friction layer resolves itself into four stages: the laminar layer, the reversal point, the turbulent layer, and the point of separation. The solution is predicated first on pressure distribution across the body surface.

Pressure Distribution

In order to solve the profile drag of a wing without resorting to measurements it must be possible also to compute the pressure distribution as it really occurs under the effect of air friction. This is not always possible to be obtained with desired accuracy. To be sure, there are methods to determine the potential theoretical pressure distribution on families of profiles (Joukowski, Karman-Trefftz, Betz-Keune (reference 16)) and even on arbitrarily shaped profiles (references 17, 18), but the measured pressure distribution are not in satisfactory agreement with those obtained by potential theory, especially at higher angles of attack. On the other hand, Betz has pointed out as far back as 1915 (reference 6) that a much better agreement could be achieved if the circulation is secured from the measured lift rather than from the condition of smooth trailing edge flow off. Admittedly, it results in flow around the trailing edge and hence in excessive low pressures. This obstacle has been removed recently by Pinkerton (reference 19) while retaining Betz' artifice, by modifying a parameter of Theodorsen's method (references 17 and 18) in somewhat arbitrary manner.

Later it will be shown that the actual pressure distribution can be obtained from the potential theory by iteration by first computing the friction layer for the potential theoretical pressure distribution and then modifying it with the aid of the computed friction layer quantities. But, in general, Pinkerton's method in conjunction with empirical values will suffice.

At small positive and negative angles of attack, however, the potential theoretical pressure distribution agrees so closely with the real to within close proximity of the trailing edge that it can be used also as a basis. At the trailing edge itself the theoretically resultant pressure rise toward the stagnation point disappears in fact (figs. 13 to 19). Therefore the pressure distribution defining the minimum value of the profile drag can be computed on slender profiles without any measurement.

Laminar Friction Layer

a) Pohlhausen Method

We employ the known method of Von Karman and Pohlhausen (reference 2) which has found two more recent and critical representations by Prandtl (reference 2) and Howarth (reference 21).

Pohlhausen expresses the velocity profile in the laminar friction layer in the form of a polynomial of the fourth rank in $\frac{n}{\delta}$:

$$u = a_0 + a_1 \frac{n}{\delta} + a_2 \left(\frac{n}{\delta}\right)^2 + a_3 \left(\frac{n}{\delta}\right)^3 + a_4 \left(\frac{n}{\delta}\right)^4$$

where n is distance from the profile and the so-called boundary layer thickness δ is defined by

$$u\left(\frac{n}{\delta}, s\right)_{n=\delta} = u_0(s) \tag{19}$$

The five coefficients of the polynomial can be obtained from the same number of limiting conditions which are secured under the usual assumption that Prandtl's boundary equation

$$u \frac{\partial u}{\partial s} + v \frac{\partial u}{\partial n} = -\frac{1}{\rho} \frac{\partial p}{\partial s} + \nu \frac{\partial^2 u}{\partial n^2} \tag{20}$$

where ρ is air density and v normal component of the velocity in the friction layer, is rigorously satisfied in points $n = 0$ and $n = \delta$. They read

$$\left.\begin{aligned} n = \delta: \quad & u = u_0; \quad \frac{\partial u}{\partial n} = \frac{\partial^2 u}{\partial n^2} = 0 \\ n = 0: \quad & u = 0; \quad \nu \frac{\partial^2 u}{\partial n^2} = -u_0 u_0' \end{aligned}\right\} \tag{21}$$

where $'$ denotes differentiation with respect to the arc length. The points $0 < n < \delta$ of the friction layer merely satisfy the Karman integral condition of the momentum (reference 20, equation 2).

$$\tau_o = \rho \frac{d}{ds} \int_o^h (u_o^2 - u^2)\, dn - \rho\, u_o \frac{d}{ds} \int_o^h (u_o - u)\, dn; \quad h \geqq \delta \tag{22}$$

which simply affords a statement about average speed values.

If the displacement thickness δ^* of the friction layer is defined by

$$\delta^* = \int_o^h \left(1 - \frac{u}{u_o}\right) dn \tag{23}$$

and the momentum thickness ϑ by

$$\vartheta = \int_o^h \left[\frac{u}{u_o} - \left(\frac{u}{u_o}\right)^2\right] dn \tag{24}$$

the Karman momentum equation can then be written in the form

$$\tau_o = \rho \frac{d}{ds} (u_o^2 \vartheta) - \delta^* \frac{dp}{ds} \tag{25}$$

From the mathematical point of view it is then appropriate to introduce a parameter λ:

$$\lambda\ (s) = \frac{u_o' \delta^2}{\nu} \tag{26}$$

which, according to Tollmien (reference 22), may be considered as quotient of the local pressure force to local friction force. From the physical point of view it would be better to form it with δ^* instead of δ.

Then the Pohlhausen velocity profile can be written in the form:

$$\frac{u}{u_o} = f\left(\frac{n}{\delta}, \lambda\right) = \frac{12 + \lambda}{6} \frac{n}{\delta} - \frac{\lambda}{2}\left(\frac{n}{\delta}\right)^2 - \frac{4 - \lambda}{2}\left(\frac{n}{\delta}\right)^3 + \frac{6 - \lambda}{6}\left(\frac{n}{\delta}\right)^4 \tag{27}$$

whence follows, if μ denotes the air viscosity, the shearing stress:

$$\tau_o = \mu \left(\frac{\partial u}{\partial n} \right)_{n=o} = \frac{\mu\, u_o (12 + \lambda)}{6\, \delta} \tag{28}$$

the displacement thickness

$$\delta^* = \delta \left(\frac{3}{10} - \frac{\lambda}{120} \right) \tag{29}$$

and the momentum thickness

$$\vartheta = \delta \left(\frac{37}{315} - \frac{\lambda}{945} - \frac{\lambda^2}{9072} \right) \tag{30}$$

Figure 4 illustrates the velocity profiles for several λ values, $\lambda = 0$ showing, according to (26) since $u_o' = 0$, the velocity distribution on the friction sheet, $\lambda = 7.052$ the velocity profile in proximity of the stagnation point. With $\lambda = -12$ is afforded, as seen from (28), the frictionless velocity profile characteristic of the breakaway of the laminar friction layer. For $\lambda < -12$ the velocity distributions manifest return flow near the wall. Alternately, if λ by great acceleration exceeds the upper limit of validity range of the Pohlhausen method, $\lambda = 12$, the result will be physically irrelevant, bulged out distributions ($\lambda = 18$).

To single out the physically nonessential boundary layer thickness δ occurring in (26) to (30), a common nonlinear differential equation must be solved, which is obtained by inserting (27) into (22). With

$$Z = \frac{\delta^2}{\nu} = \frac{\lambda}{u_o'} \tag{31}$$

this differential equation reads

$$\frac{dZ}{ds} = \frac{f(\lambda)}{u_o} + Z^2\, u_o''\, g(\lambda) \tag{32}$$

where

$$f(\lambda) = \frac{7257.6 - 1336.32\,\lambda + 37.92\,\lambda^2 + 0.8\,\lambda^3}{213.12 - 5.76\,\lambda - \lambda^2} \tag{33}$$

and $$g(\lambda) = \frac{3.84 + 0.8\,\lambda}{213.12 - 5.76\,\lambda - \lambda^2} \qquad (34)$$

The functions $f(\lambda)$, $g(\lambda)$ have been tabulated by Howarth (reference 21) for the $-12 \leq \lambda \leq +12$ validity range of the method. After defining u_o' and u_o'' by graphical or numerical differentiation, the isoclinic field $\frac{dZ}{ds} = \text{const}$ can be plotted and in it the integral curve $Z(s)$, if the stagnation point conditions are observed, for a given pressure distribution along the profile and hence a given velocity distribution $u_o(s)$. If $Z(s)$ meets the curve $Z_a(s) = -\frac{12}{u_o'}$ at a certain $s = s_a$, the separation of the laminar friction layer takes place in this profile point.

From $Z(s)$ follows, according to (31), the boundary layer thickness $\delta(s)$ and hence, according to (26), (28) (29), (30), the characteristic quantities λ, τ_o, δ^*, and ϑ of the laminar boundary layer. A noticeable fact is that the dimensionless λ is a characteristic value for every profile point, independent of $\mathrm{Re} = \frac{u_\infty t}{\nu}$, if the pressure distribution over the wing contour is independent of Re, as is the case in the customary test and flight conditions. On replacing λ for Z in (32) a differential equation for λ independent of Re results. It follows particularly that the position of the breakaway ($\lambda = -12$) of the laminar friction layer is independent of Re.

It further follows from this irrelation that the boundary layer thickness δ_1 and δ_2 related to two different Reynolds numbers $\mathrm{Re}_1 = \frac{u_{\infty 1}\, t_1}{\nu_1}$ and $\mathrm{Re}_2 = \frac{u_{\infty 2}\, t_2}{\nu_2}$ are associated through

$$\lambda = \frac{u_{o1}'\,\delta_1^2}{\nu_1} = \frac{u_{o2}'\,\delta_2^2}{\nu_2} = \text{const}, \qquad (35)$$

or

$$\frac{\delta_1}{\delta_2} = \frac{t_1}{t_2}\sqrt{\frac{\mathrm{Re}_2}{\mathrm{Re}_1}} \qquad (36)$$

By leaving t and ν constant while varying the flying speed u_∞,

$$\frac{\delta_1}{\delta_2} = \sqrt{\frac{u_{\infty 2}}{u_{\infty 1}}} \qquad (37)$$

can be used to reduce the quantities τ_0, δ^*, ϑ, of one speed for which they were computed with the help of the fairly cumbersome isoclinic method to another flying speed.

b) Note on the Pohlhausen Method

The usefulness of the Pohlhausen approximate method is substantially enhanced by the fact that it affords, on the friction sheet, good agreement with the exact Blasius method and on the circular cylinder with Hiemenz' measurements. More recently, Schubauer (reference 23) measured the laminar boundary layer on an elliptic cylinder of major and minor axis $a_1 = 0.299$ meters and $a_2 = 0.101$ meters, respectively, by means of a hot wire anemometer. The direction of the impinging air stream was parallel to the major axis, the air speed $u_\infty = 35$ meters per second. Schubauer obtains from stagnation point $\frac{s}{a_2} = 0$ to $\frac{s}{a_2} = 1.832$ very good agreement in speed distributions with Pohlhausen's figures, but encounters no separation, theoretically, for higher values of $\frac{s}{a_2}$, whereas the experiment itself indicates separation at $\frac{s}{a_2} = 1.99$. Schubauer draws the conclusion that the Pohlhausen method is unsuitable by small pressure rise for computing the separation point when this pressure rise does not last long. This inference is, however, inconsequential for our laminar friction layer on the wing; in the first place, the laminar layer will sooner or later turn turbulent anyhow, before it separates and, in the second place, the pressure rise lasts over a much greater distance than on the elliptic cylinder. The good agreement of the velocity profiles in the laminar friction layer with those computed by Pohlhausen, on the contrary justifies the use of this method on the wing also.

The question suggests itself whether the quality of the velocity profile could be improved with a polynomial of higher than fourth order and its coefficient secured with the aid of further boundary conditions. A more accurate computation shows that a polynomial of the sixth order gives the shearing stress on the friction sheet to within 1/2 percent exactness, that of the fourth order only to within $3\frac{1}{2}$ percent. With polynomials higher than the sixth order, the coefficients cease to be linear functions of λ. Because the subsequent boundary conditions on the wall are then accompanied by differential quotients of the coefficients with respect to s, With every such condition containing the derivation of a new coefficient in respect to s, the order of the differential equation for δ rises. On top of that, the amount of paper work involved herewith imposes a limit to the use of polynomials of higher order which cannot be exceeded even by foregoing the compliance of higher boundary conditions on the walls and by satisfying only those on the boundary layer limit. By these contiguities of higher order on the border of the friction layer the velocity profile becomes much more complete than it actually is.

Whether the polynomials of higher order reproduce the actual velocity profile in every laminar friction layer better than those of lower order is itself difficult to decide as long as the convergence of this method is not proved.

Attempts might be made to find out whether formulas for the velocity profile other than the polynomial in $\frac{n}{\delta}$ would give more comprehensive agreement with the experiment. Kosmodemiansky's attempt (reference 24)

$$\frac{u}{u_o} = P\left(\frac{n}{\delta}\right) \sin\left(\frac{\pi}{2}\frac{n}{\delta}\right) \tag{38}$$

where $P\left(\frac{n}{\delta}\right)$ is again a polynomial does not lead any farther.

So for the time being there is no known method for computing the laminar boundary layer by selected pressure distribution that is definitely superior to the Pohlhausen method.

One simplification of the latter's method which may be of some advantage in cursory computations might be

pointed out: namely, for a special class of pressure distributions the solution $\delta(s)$ can be numerically given without plotting of the isoclinic field. If

$$\frac{u_o\, u_o''}{u_o'^2} = C = \text{const} \tag{39}$$

the variables for λ in (32) can be separated. It affords, according to Golubew (reference 25),

$$\frac{d\,u_o}{u_o} = \frac{p(\lambda)d\lambda}{q(\lambda) + C\, r(\lambda)} \tag{40}$$

$p(\lambda)$, $q(\lambda)$, $r(\lambda)$ being represented by the rational functions

$$\left.\begin{aligned} p(\lambda) &= -213.12 + 5.76\,\lambda + \lambda^2 \\ q(\lambda) &= -7257.6 + 1336.32\,\lambda - 37.92\,\lambda^2 - 0.8\,\lambda^3 \\ r(\lambda) &= -213.12\,\lambda + 1.92\,\lambda^2 + 0.2\,\lambda^3 \end{aligned}\right\} \tag{41}$$

Integration of (39) affords the class of the plotted potential velocity distributions at

$$u_o(s) = c_2\left[(1 - C)s + c_1\right]^{\frac{1}{1-C}} \quad \text{for} \quad C \neq 1 \tag{42}$$

and

$$u_o(s) = c_2 e^{s/c_1} \quad \text{for} \quad C = +1 \tag{43}$$

The integration constants c_1 and c_2 are defined by the initial conditions

$$u_o(s_o) = u_{oo} \quad \text{and} \quad u_o'(s_o) = u_{oo}'$$

For $C = 0$ and $c_1 = 0$, it affords the stagnation point flow; for $C = -1$, the flow with constant pressure gradient; for $C = +1$ and $c_1 \to \infty$, the flow on the friction layer.

A more careful consideration shows that it does not suffice to replace a predetermined pressure distribution by a polygon of straight pieces of $\frac{dp}{ds} = \text{const}$ $(C = -1)$.

Approximating it by arcs of curves on which C has momentarily a different value involves just as much paper work as the plotting of the isoclinic field. So in order to gain a somewhat clearer insight into the laminar boundary layer on the wing the isoclinic field of the Pohlhausen method can hardly be spared at present.

The Transition Point

According to Pohlhausen the friction layer on a wing can be computed as it would occur if it were laminar up to the trailing edge or at least as far as its separation point.

But this assumption is complied with only at small Reynolds numbers seldom encountered in practical flight. In reality the laminar layer becomes turbulent before reaching its separation point. When, as on the friction sheet (fig. 3) the transition is assumed to occur abruptly in a point, the cardinal question of the entire profile drag computation arises: namely, where is this transition point located. The reason the problem of theoretical location of the point is so difficult is due to the fact that it belongs within the ambit of turbulence origin altogether. Since, even on the friction sheet in nonvortical flow the transition point defies computation on the basis of theoretical considerations, the chances of accomplishing it in an airstream with a certain turbulence and accompanied by a pressure gradient over the arc length of the body are even less. Qualitatively it might be expected that a high turbulence factor produces an earlier transition because at least the boundary regions are more strongly intermingled and hence the laminar friction layer is made turbulent from the outside. It is also suspected that, under identical conditions otherwise, a greater pressure rise promotes an earlier transition, since it leads to unstable velocity profiles, that is, those with ascending return flow risks, and so makes the laminar friction layer turbulent from the inside, from the wall. Besides, the position of the transitional point is dependent upon $Re = \frac{u_\infty t}{\nu}$, as is known from the friction sheet (equation (5)).

The pressure distribution over a wing at constant angle of attack in a flow of different air speed is practically independent of the Reynolds number in both the subcritical and the supercritical range. At very small

Reynolds numbers the friction layer is laminar until — only by greater pressure rise toward the trailing edge — it separates in a point, the location of which is independent of Re. If the Reynolds number continues to increase the friction layer becomes turbulent shortly before the separation point is reached at a critical Reynolds number $Re_k = \frac{u_{\infty k} t}{\nu}$, which, besides the wing shape, is dependent on the turbulence of the air stream. Transition point and laminar separation point coincide. The profile drag coefficient drops abruptly because the dead air region and hence the pressure drag is reduced by the adherence of the turbulent friction layer beyond the laminar separation point. On further increase in Re the transition point travels forward toward pressure minimum. That it can advance even before the pressure minimum has been only rarely and somewhat uncertainly observed; but perhaps merely the Reynolds numbers in the past test and flight conditions are still too small to produce such an effect.

For the usual range of Reynolds numbers therefore, it may be said that the transition point lies between laminar separation point and pressure minimum. Sharper criteria can be expected only on the basis of measurements at different pressure gradients and turbulence factors, which are still lacking for the present in sufficient quantities.

Gruschwitz (reference 26) defined the transition point in his plate measurements in the pressure field and on the Göttingen standard airfoil section no. 387 by plotting the quotient $\frac{u(\vartheta)}{u_o}$ against the arc length, and located the transition point where this quotient showed a sudden steep rise. On the basis of his experiments he found that the Reynolds number

$$Re_\vartheta = \frac{u_o \vartheta}{\nu} \tag{44}$$

formed with the laminar momentum thickness ϑ should, for the transition point, lie in the region

$$360 < Re_\vartheta < 680 \tag{45}$$

Schmidbauer (reference 27) found

$$500 < Re_{\delta^*} < 790 \tag{46}$$

on curved surfaces, and

$$500 < Re_{\delta} < 550 \tag{47}$$

for the specific case where the transition point is exactly located in the laminar separation point. Peters (reference 28), on the other hand, obtained the narrow interval

$$600 < Re_{\delta} < 650 \tag{48}$$

for the transition point on a symmetrical wing of 16.6 percent thickness. Rewriting the transition criterion (5) for the flat plate to Re_{δ}, affords

$$Re_{\delta} = \frac{u_{\infty}\,\delta}{\nu} = 460 \tag{50}$$

since the momentum thickness on the friction sheet is, according to Blasius:

$$\delta = 0.75\sqrt{\frac{\nu x}{u_{\infty}}} \tag{49}$$

Dryden (reference 29) supposes on the basis of his experiments that on the friction sheet the transition criterion for 0.5 percent turbulence can be raised to $Re_{\delta} = 680$ and for 3 percent turbulence, lowered to $Re_{\delta} = 210$. The criterion (50) is located approximately in the center of Dryden's range.

Fage's experiments (reference 30) on Reynolds numbers in the transition point included circular cylinder, airfoil section, sphere, and flat plate. He defined the transition point as the place of minimum laminar skin friction (fig. 3). This definition is identical with that by Gruschwitz. Fage, considering only the behavior of the shearing stress as essential for the character of flow and foregoing the determination of the exact form of the velocity profile, could confine his measurements to the wall adjacent region with linear velocity increase rather than over the total friction layer width. He formed the Reynolds number of the friction layer with the displacement thickness δ^* instead of with the momentum thickness δ and found that

$$Re_{\delta}^{**} = \frac{u_o^* \delta^*}{\nu}; \qquad u_o^* = \sqrt{\frac{\tau_o}{\rho}} \tag{51}$$

was not very dependent upon the body form and increased slightly with decreasing turbulence. Another noteworthy fact is that Fage established a definite inflection in the pressure distributions along the body contour on the transition point, so that the transition point can be experimentally secured without friction layer measurement by a very careful pressure distribution measurement.

From the widely divergent range of Re_{ϑ} (fig. 5) it is apparent that the location of the transition point can be given as yet with very little assurance. So for the time being at least the profile drag of a wing at a given Reynolds number $Re = \frac{u_\infty t}{\nu}$ should be computed for several transition points, which means, compute $Re_{\vartheta}(s)$ with the aid of the laminar momentum thickness defined according to Pohlhausen, and select arbitrarily several transition points s_u from, say, the Gruschwitz range. These transition points are the starting points of the turbulent friction layer.

The Turbulent Friction Layer

a) Gruschwitz' Method

The turbulent friction layer is computed by the approximate method proposed by Gruschwitz (reference 26). Like Pohlhausen in his method for laminar friction layer, Gruschwitz starts with the Karman momentum equation (reference 25); but rather than the velocity distribution itself he simply characterizes it by a form parameter η:

$$\eta = 1 - \left[\frac{u(\vartheta)}{u_o}\right]^2 \tag{52}$$

One difference existing between the laminar form parameter λ and the turbulent form parameter η is that λ as analytical function of pressure gradient and friction layer measurement is theoretically predictable while the calculation of η dictates other empirical laws.

Since it is necessary to forego an analytical formula

for the turbulent velocity profile, the calculation of the four friction-layer quantities η, τ_0, δ^*, and ϑ calls for four relations between these four variables.

The first represents Karman's momentum equation (25) which, rewritten, reads:

$$\frac{\tau_0}{\rho u_0^2} = \frac{d\vartheta}{ds} + \left(1 + \frac{1}{2}\frac{\delta^*}{\vartheta}\right)\frac{\vartheta}{u_0^2}\frac{d u_0^2}{ds} \tag{53}$$

A second relation is afforded by the function

$$H(\eta) = \frac{\delta^*}{\vartheta} \tag{54}$$

obtained by Gruschwitz from the evaluation of the recorded turbulent velocity profiles (fig. 6).

The third relation was obtained by Gruschwitz from another equation deduced from his experimental data. He reasoned that the energy change of a fluid particle, moving at distance $n = \vartheta$ from the wall, must certainly be dependent on $u(\vartheta, s)$, $u_0(s)$, $\vartheta(s)$, and ν. From dimensional considerations the following form is suggested,

where $q = \frac{\rho}{2} u_0^2$:

$$\frac{\vartheta}{q}\frac{d}{ds}\left[\frac{\rho}{2}\overline{u^2(\vartheta)} + p\right] = -\frac{\vartheta}{q}\frac{d}{ds}(q\,\eta) = F(\eta, Re_\vartheta) \tag{55}$$

From his measurements Gruschwitz found that the dependence of Re_ϑ was negligibly small and the dependence of η on $\eta = 0.8$ expressible by a linear law:

$$\frac{\vartheta}{q}\frac{d}{ds}(q\,\eta) = -0.00894\,\eta + 0.00461 \tag{56}$$

With the abbreviation

$$q\,\eta = \xi \tag{57}$$

where ξ indicates the dynamic pressure difference on the friction layer boundary and on δ, equation (56) can also be written in the form

R.T.U.

$$\frac{d\xi}{ds} = - 0.00894\,\xi + 0.00461\,q \qquad (58)$$

The fourth equation is lacking for the time being; hence an estimation of τ_o is substituted.

With (53), (54), and (58) the quantities ϑ, η, δ^* can then be approximately computed as follows:

Karman's momentum equation (53) is interpreted as differential equation for ϑ. Posting constant mean values for $\frac{\tau_o}{\rho u_o^2}$ and $H = \frac{\delta^*}{\vartheta}$ and assuming as initial momentum thickness of the turbulent friction layer that having the laminar friction in the transition point the differential equation for ϑ from the transition point can be graphically integrated by a method originating with Czuber and described by Gruschwitz. Gruschwitz found

$$\frac{\tau_o}{\rho u_o^2} = 0.002; \quad H = 1.5 \qquad (59)$$

as acceptable approximation.

The first approximation for ϑ is entered in (58) for ξ, which is solved by the same method, by starting according to Gruschwitz, in the transition point with $\eta = 0.1$, that is, $\xi = 0.1\,q$. This value of η in the transition point is arbitrary to a certain extent; above all, it corresponds in no manner to the experimental finding according to which the turbulence ordinarily starts at high η values. Gruschwitz found, however, that with $\eta = 0.1$ the theoretical and experimental η curves agreed best at some distance from the transition point; for the rest, a change in initial value does not amount to much because of the marked convergence of the curves. According to (57) then $\eta(s)$ is obtained from $\eta(s)$.

Reading off the values of H for η from figure 6, affords according to (54) the displacement thickness δ^*. This then would leave the shearing stress determination in the turbulent boundary layer with the aid of a fourth relation between quantities δ^*, ϑ, η, and τ_o, which has not been found to the present time. Gruschwitz therefore attempted to define the shearing stress

in the following manner: On the assumption of the 1/7 power law for the velocity distribution in the turbulent friction layer

$$\frac{u}{u_0} = \left(\frac{n}{\delta}\right)^{1/7} \tag{60}$$

in flows without pressure gradient, that is, on the friction sheet ($u_0 = u_\infty$), the shearing stress τ_0 can be represented in the form:

$$\frac{\tau_0}{\rho u_0^2} = 0.0225 \left(\frac{\nu}{u_0 \delta}\right)^{1/4} = 0.0225 \, Re_\delta^{1/4} \tag{61}$$

Then

$$\delta^* = \frac{1}{8} \delta \qquad \frac{9}{72} \tag{62}$$

$$\vartheta = \frac{7}{72} \delta \qquad H = \frac{9}{7} = 1.286 \tag{63}$$

according to (23), (24), and (60), whence we can also write:

$$\frac{\tau_0}{\rho u_0^2} = 0.01338 \, Re_{\delta^*}^{-1/4} = 0.01256 \, Re_\vartheta^{-1/4} \tag{64}$$

Gruschwitz then proceeded to compute the shearing stress $\tau_0(s)$ in a turbulent friction layer by arbitrary pressure gradients, according to (64), where he entered $u_0(s)$ and the first approximation of $\vartheta(s)$ in this equation.

It needs to be proved why and under what restrictive conditions this method is justified. Nikuradse (reference 31) evolved an empirical relation between pressure gradient and shearing stress from his measurements in water flows with different pressure gradients (wedge flow with varying included angle). He found that the speed distribution could be characterized by a "form parameter"

$$\Gamma_1 = -\frac{\delta^*}{u_0} \frac{d u_0}{ds} \left(\frac{u_0 \delta^*}{\nu}\right)^{1/4} = -\frac{\delta^*}{u_0} \frac{d u_0}{d s} Re_{\delta^*}^{1/4} \tag{65}$$

Figure 7 illustrates the relation of the dimensionless coefficient of the shearing stress

$$T_1 = \frac{\tau_0}{\rho u_0^2} (Re_{\delta *})^{1/4} \qquad (66)$$

with this dimensionless parameter Γ_1. It will be seen that T_1 increases a little at first with increasing Γ_1 in delayed flow ($\Gamma_1 > 0$), but then drops rapidly. Gruschwitz' application of the boundary layer law (64) to flows with pressure gradients is obviously therefore justified for points on the wall on which Γ_1 departs so little from zero that $T_1(\Gamma_1)$ still closely approaches the value $T_1(0)$ on the friction sheet. In proximity of the region of separation ($T_1 = 0$) this method therefore fails.

In any event, Nikuradse's function $T_1(\Gamma_1)$ affords a satisfactory substitute for the still lacking fourth condition between quantities δ^*, ϑ, η, and τ_0, thus enabling the solution of these four factors of the turbulent friction layer on the wing.

b) Comparison of the Gruschwitz' Method with Experiment

This is to be a brief examination of the extent of agreement of the Gruschwitz approximate solution with the measurements on turbulent friction layers. He himself checked his theory first on his own friction layer measurements made on the flat plate in the pressure field and on a Göttingen airfoil section no. 387. The measurements the evaluation of which he reported in his article were carried out in the range $8.5 \times 10^5 < Re < 2.6 \times 10^6$. But he also compared his theory with the Fage and Falkner tests (reference 32) on a symmetrical Karman–Trefftz profile of 15 percent thickness, at $Re = 1.7 \times 10^6$. The η curves agreed closely on the whole; but the theoretical ϑ curve on the Karman–Trefftz profile afforded too high values toward the trailing edge, while on the plate the theoretical and experimental ϑ curves manifested coincidence in the pressure field.

Stüper (reference 33) was able to confirm Gruschwitz' solution in flight tests at $2.82 \times 10^6 < Re < 4.88 \times 10^6$, and with the same approximate values for $\frac{\tau_0}{\rho u_0^2}$ and H. But here also the theoretical ϑ curve toward the trailing edge seems to lie on the whole above the experimental value.

Peters (reference 28) exploring the friction layer on a symmetrical airfoil of 2.3 meters chord in his check of Gruschwitz' theory at larger Reynolds numbers also achieved very good agreement at small positive and negative angles of attack, on the basis of the approximate values (equation 59):

$$\frac{\tau_o}{\rho\, u_o^2} = 0.0017; \quad H = 1.4 \tag{67}$$

The lower value of the shearing stress is evidently chosen because of the larger Reynolds number the amount of which is not given.

As approximate value for the shearing stress by a given Re the mean shearing stress $\overline{\tau_o}$ of the friction sheet at the same Reynolds number $Re = \frac{u_\infty t}{\nu}$ is generally accepted.

$$\frac{\overline{\tau_o}}{\rho\, u_o^2} = \frac{c_w}{4} \tag{68}$$

c_w being computed from (4) or (6) depending upon the character of flow.

But Peters' report also discloses the same systematic departing of the Λ curves toward the trailing edge by increasing angle of attack, which for the moment cannot be explained; for the approximate value of $\tau_o/\rho\, u_o^2$ plays precisely in the rear part of the wing where the pressure gradient is great, no decisive part; on the other hand, the wing itself remains sufficiently flat, so that Schmidbauer's curvature effect (reference 27) can be discounted.

A further unusual fact is that Gruschwitz' $H(\eta)$ curve was confirmed by Schmidbauer as well as Peters. This is easy to understand since curve $H(\eta)$ represents a purely geometrical relationship.

Relations between the Parameter Shape of Laminar and Turbulent Velocity Profiles

This geometric character is seen from the following:

In many cases the speed distribution in the turbulent boundary layer has, while discounting direct wall proximity where a laminar sublayer with finite shearing stress is formed, approximately the form of a power law:

$$\frac{u}{u_0} = \left(\frac{\eta}{\delta}\right)^k ; \quad k = 1/6,\ 1/7,\ 1/8 \tag{69}$$

Then function $H(\eta)$ must be given explicit. Because it is, according to (23) and (24):

$$\frac{\delta^*}{\delta} = \frac{k}{k+1} \tag{70}$$

$$\frac{\vartheta}{\delta} = \frac{k}{(k+1)(2k+1)} \tag{71}$$

and

$$H = \frac{\delta^*}{\vartheta} = 1 + 2k \tag{72}$$

or

$$k = \frac{H-1}{2} \tag{73}$$

whence, according to (52), the form parameter:

$$\eta = 1 - \left(\frac{\vartheta}{\delta}\right)^{2k} = 1 - \left[\frac{H-1}{H(H+1)}\right]^{H-1} \tag{74}$$

This function $\eta(H)$, plotted in figure 6, varies very little from the Gruschwitz experimental curve.

Because of its geometric nature the relation $H(\eta) = \frac{\delta^*}{\vartheta}$ is not tied to the flow character in the friction layer and can therefore be applied also to the laminar friction layer. According to the friction layers plotted by the Pohlhausen method in figure 6 the parameter η varies little from 1 throughout the laminar range and is therefore not properly suited for representation of the laminar speed distributions. Gruschwitz and Schmidbauer both secured η values of the order of magnitude of Pohlhausen's in the cases where laminar friction layer profiles were measured.

The Point of Separation

Under a strong pressure rise it may happen that the turbulent friction layer does not adhere as far as the trailing edge but separates before. Gruschwitz adduced the separation criterion

$$\eta = 0.8 \tag{75}$$

while Schmidbauer suspected that the separation risk is postponed to $\eta \sim 0.9$ on the assumption that the pressure rise at high η is flat. Peters' findings comply very closely with the Gruschwitz separation criterion (75), if the η values secured from the measured speed distributions are used as a basis. The theoretical solution of η, however, affords inferior values in proximity of the separation point; hence no separation is at all predictable therefrom.

Gruschwitz likewise associated the location of the separation point with that of the transition point. The earlier the transition takes place the greater becomes the turbulent boundary layer thickness in a fixed profile point behind the transition point. And this is accompanied by a greater risk of separation; hence at constant $\mathrm{Re} = \frac{u_\infty t}{\nu}$ the separation point $\eta = 0.8$ moves forward when the transition point is shifted forward. By fixed transition point and ascending Reynolds number, on the other hand, the separation region shifts toward the trailing edge because the momentum thickness becomes less. These two effects are superimposed on the wing in such a way that the effect of the Reynolds number on the separation point follows as the difference of two effects, the prefix of which does not appear to be absolute. At small and medium Reynolds numbers the effect of transition point travel usually preponderates, that is, with ascending Reynolds number the transition point shifts forward, the drag increases. But, when at larger Reynolds numbers the transitional region is already far forward so that its location can be looked upon as approximately constant, the first effect disappears and the separation point shifts backward with ascending Reynolds number, the drag decreases.

Nikuradse (see fig. 7) also secured a separation criterion from his experiments, at least by extrapolation:

$$\Gamma_1 = 0.08 \tag{76}$$

which is in good agreement with the Gruschwitz criterion, as will be shown later.

Since the dynamical effect of the dead air region is to be disregarded, we possess herewith the theoretical means to compute the friction layer from stagnation point to separation point or on thin profiles as far as the trailing edge.

IV. METHOD OF PREDICTING THE PROFILE DRAG FROM THE CHARACTERISTICS OF THE FRICTION LAYER

1. Friction Drag

The friction drag is determined according to (1) by the variation of the shearing stress τ_0, which itself is a characteristic quantity of the friction layer.

Karman's momentum equation (25) represents a general relation between τ_0, δ^*, and ϑ. If the two characteristic lengths δ^* and ϑ could be computed without recourse to the Karman equation, this would afford the possibility of computing the shearing stress and so, the friction drag. Integration of the shearing stress resulting from the Karman momentum equation along the profile surface gives the friction drag per unit length of span:

$$W_r = \int_{I+II} \tau_0 \cos\beta \, ds = \rho[u_0^2 \vartheta \cos\beta]_{I+II} - \int_{I+II} \delta^* \frac{dp}{ds} \cos\beta \, ds \tag{77}$$

The subscripts under the integral signs again denoting integration from stagnation point with respect to suction side and pressure side, and the subscripts on the square brackets the corresponding values of the bracketed trailing edge term.

In the laminar friction layer the shearing stress can be approximated by the Karman–Pohlhausen method. But in the turbulent layer where only equations (53), (54), and (58) are available for defining δ^*, ϑ, η, and τ_0, an estimation of the shearing stress τ_0 has to serve as fourth equation. For the solution of ϑ and δ^* the uncertainty of τ_0 plays no great part, since these quan-

tities generally are not very dependent on τ_0, but in the determination of the friction drag the uncertainty of the τ_0 appraisal is significant according to equation (64). A reliable solution of τ_0 and hence of the profile drag could be secured if τ_0 could be tied in with the form parameter η, as on the laminar friction layer.

2. Pressure Drag

The pressure drag of a wing has been determined up to now by plotting — according to (2) — the pressure p against the coordinate z of the profile points normal to the direction of flight and defining the area of this pressure distribution. However, as has been pointed out by Betz (reference 6), the theoretical uncertainty of this method is that this area consists of comparatively large positive and negative parts, as a result of which the pressure drag is obtained as difference of two doubtful values of the same order of magnitude. This defect has been subsequently substantiated from various sources (references 34 and 35).

A method is therefore developed which is amenable to the theoretical solution from the friction layer quantities and obviates this uncertainty. Strictly speaking, we confine ourselves to the case where no separation occurs in the friction layer; hence the pressure drag is exclusively due to the fact that the adhering friction layer pushes the potential flow away from the surface to the amount of the displacement thickness δ^*. But if separation occurs, the effects of these separated air balls on the wing must be taken into consideration, according to Betz (36). As long as the separation is insignificant, these reactions are minor and the pressure drag can then still be estimated, at least approximately.

The line of reasoning of this method is as follows (fig. 8):

Visualize a flow past the surface which is frictionless, but with the same displacement of streamlines in relation to potential flow as occurs on the natural friction-encumbered flow. This displacement is effected by superposing a source on the surface. With this superposition of source flow on the original potential flow a new potential flow with the same pressure distribution as the actual flow is obtained.

The control area on which the force equilibrium is to be analyzed, is then defined as follows: Place a skin G at equal distance δ^* around the wing T, δ^* itself being defined by (23). This skin represents, as it were, the surface of the displacement water through which no fluid of the source flow passes any longer. On the trailing edge this skin is closed off by a plane H at right angle to the direction of flight. The pressure and momentum on the closed control area formed by T, G, and H are now analyzed. With D denoting the resultant in flight direction stemming from the pressure forces and that produced by the momentum with I, must follow:

$$D_T + I_T + D_G + I_G + D_H + I_H = 0 \qquad (78)$$

Area G having been chosen so that no momentum passes through, it is therefore

$$I_G = 0 \qquad (79)$$

whence the pressure drag of the wing follows at:

$$-D_T = D_G + D_H + I_H + I_T \qquad (80)$$

The solution of the momentum entering through the wing surface and plane H at the trailing edge must be preceded by the determination of the source superposition on the wing surface. At a selected point $s = s_o$ of the wing profile the fluid volume $u_o\delta^*$ is displaced per unit length of span per unit time. At $s = s_o + ds$ this volume amounts to $u_o\delta^* + \frac{d(u_o\delta^*)}{ds} ds$. Hence the displacement by the friction layer per unit time is greater by $\frac{d(u_o\delta^*)}{ds}$ at $s = s_o + ds$ than at point s_o. This fact can be interpreted as if on line $s = s_o$ in span direction a source had been superposed with a yield per unit length of span of:

$$dE = \frac{d(u_o\delta^*)}{ds} ds \qquad (81)$$

Hence the momentum per unit time entering at $s = s_o$, the region bounded by T, G, and H, amounts to

$$dI_T' = -\rho u_o d E = -\rho u_o \frac{d(u_o\delta^*)}{ds} ds \qquad (82)$$

where entering impulses are negative, transported impulses are positive. The total impulse passing through the wing surface is

$$I_T' = -\rho \int_{I+II} u_o \frac{d(u_o \delta^*)}{ds} ds \tag{83}$$

and its component in flight direction

$$I_T = -\rho \int_{I+II} u_o \frac{d(u_o \delta^*)}{ds} \cos \beta \, ds = -\rho \int_{I+II} u_o \frac{d(u_o \delta^*)}{ds} dx \tag{84}$$

Through the plane at the trailing edge the momentum

$$I_H' = \rho [u_{o_{H_I}} E_I + u_{o_{H_{II}}} E_{II}] = \rho [u_o E]_{I+II} \tag{85}$$

is transported, where $u_{o_{H_I}}$, $u_{o_{H_{II}}}$ are the potential velocities at the trailing edge on suction and pressure side and E_I, E_{II} the corresponding source yields:

$$\left.\begin{aligned} E_I &= \int_I \frac{d(u_o \delta^*)}{ds} ds = u_{o_{H_I}} \delta^*_{H_I} \\ E_{II} &= \int_{II} \frac{d(u_o \delta^*)}{ds} ds = u_{o_{H_{II}}} \delta^*_{H_{II}} \end{aligned}\right\} \tag{86}$$

Its component in flight direction is

$$I_H = \rho [u_{o_H}^2 \delta_H^* \cos \beta_H]_{I+II} \tag{87}$$

with β_{H_I}, $\beta_{H_{II}}$ denoting the angle between profile tangent and flight direction at the trailing edge.

In order that the pressure drag D_T may be computed, the pressure force on area G and plane H must be defined. The first follows from Bernoulli's equation at

$$D_H = \frac{\rho}{2} [(u_\infty^2 - u_{o_H}^2 \cos \beta_H) \delta_H^*]_{I+II} \tag{88}$$

The second from the argument: The continuation of area G placed at distance δ^* around the wing, beyond the trailing edge as area S so that its width is everywhere equal to the displacement thickness δ^* of the dead-air region, does not alter the potential flow outside this surface nor, hence, the pressure distribution. However, G and S represent a so-called conoid on which the resultant pressure force of a potential flow is known to be zero, that is, it affords $D_G + D_S = 0$ or

$$D_G = - D_S \tag{89}$$

With $2\delta^*$ (see footnote) denoting the width of the wake body at any point and p the pressure, the pressure force in the wake flow becomes

$$D_S = 2 \int_{\delta_H^*}^{\delta_\infty^*} p \, d \, \delta^* \tag{90}$$

where $2 \delta_\infty^*$ is the displacement thickness for $u_o = u_\infty$.

Therefore the displacement thickness in the wake with respect to the outside pressure must be established. It can be assumed approximately that over the short distance in which the pressure abates to its final value, no appreciable energy changes take place in the wake, so that each particle is merely subject to the acceleration due to the pressure differences. Then to each stream filament Bernoulli's equation

$$\frac{\rho}{2}(v^2 - u_H{}^2) = \frac{\rho}{2}(u_o{}^2 - u_{o\,H}{}^2) = p_H - p \tag{91}$$

can be applied and hence the wake configuration u(n) at every other place in relation to the prevailing pressure computed from the velocity profile at the trailing edge $u_H(n_H)$.

The velocity profile in the friction layer at the trailing edge might be approximated by the power law

$$u_H = u_{o\,H}\left(\frac{n_H}{\delta_H}\right)^k \tag{92}$$

It is $2\delta^* = \delta_I{}^* + \delta_{II}{}^*$, where $\delta_I{}^*$, $\delta_{II}{}^*$ indicate the proportions of the wake displacement thickness, emanating from the friction layer flows at suction and pressure side; on the trailing edge itself $2\delta_H{}^* = \delta_{H_I}{}^* + \delta_{H_{II}}{}^*$.

To simplify matters, it is assumed that the flow is almost symmetrical, that is, the same on pressure side and suction side. The exponent k and the boundary layer thickness δ_H follow from the displacement thickness δ_{H*} and the momentum thickness ϑ on the trailing edge, according to (70) and (73).

Equations (91) and (92) afford first the wake velocity on a stream filament which on the trailing edge is by n_H distant from the wing surface.

$$u = \sqrt{u_o^2 - u_{o\,H}^2 + u_H^2} = u_{o\,H} \sqrt{\left(\frac{u_o}{u_{o\,H}}\right)^2 - 1 + \left(\frac{n_H}{\delta_H}\right)^{2k}} \qquad (93)$$

By given u_o it affords in the center of the wake body $(n = n_H = 0)$:

$$u_m = u_{o\,H} \sqrt{\left(\frac{u_o}{u_{o\,H}}\right)^2 - 1} \qquad (94)$$

The general coordination of n and n_H, which first defines the velocity profile $u(n)$ and then the displacement thickness δ^* of the wake, is found in the continuity equation:

$$u \, d\, n = u_H \, d\, n_H \qquad (95)$$

when starting from $n = 0$, we proceed step by step from one streamline to the next.

For $k = 1$ and $k = 1/2$, $u(n)$ can even be obtained by squaring. With the abbreviation

$$\frac{u_o}{u_{o\,H}} = \gamma \qquad (96)$$

equation (95) gives for $k = 1$:

$$\frac{u}{u_{o\,H}} = \frac{n}{\delta_H} + \sqrt{\gamma^2 - 1} \qquad (97)$$

$$\frac{\delta^*}{\delta_{H^*}} = \frac{1}{\gamma} - 2\sqrt{\gamma^2 - 1} + 2\sqrt{\gamma^2 + \frac{1}{\gamma^2} - 2} \qquad (98)$$

and for $k = 1/2$:

$$\frac{n}{\delta_H} = \frac{u}{u_o H}\sqrt{\frac{u^2}{u_o H^2} - \gamma^2 + 1} - (\gamma^2 - 1)\ln\left[\frac{1}{\sqrt{\gamma^2 - 1}}\left(\sqrt{\frac{u^2}{u_o^2 H} - \gamma^2 + 1} + \frac{u}{u_o H}\right)\right] \quad (99)$$

The curve of half the wake body width $\frac{\delta^*}{\delta_H^*}$ is shown plotted against γ for $k = 1$, $1/2$, $1/4$, and $1/8$ in figure 9.

Furthermore, with the pressure in the section of width $2\delta^*$ at

$$p = \frac{\rho}{2}(u_\infty^2 - u_o^2) = \frac{\rho}{2} u_\infty^2\left[1 - \left(\frac{u_o H}{u_\infty}\right)^2 \gamma^2\right] \quad (100)$$

the pressure drag D_S exerted on the wake follows from (90) at:

$$D_S = 2\int_{\delta_H^*}^{\delta_\infty^*} p\, d\,\delta^* = \rho\, u^2\, \delta_H^*\, Q\left(k, \frac{u_o H}{u_\infty}\right) \quad (101)$$

Factor Q is illustrated in figure 10. Exponent k corresponds to Gruschwitz' parameter η because of (74), according to the table:

k	1	1/2	1/4	1/8
η	0.973	0.833	0.633	0.454

Hence, with the integral in I_T partially integrated and angle β disregarded, equations (80), (84), (87), (88), (89), and (101) give the pressure drag at

$$D_T = W_d = \int_{I+II} \delta^* \frac{dp}{ds}\, dx + \rho\, u_o H^2\, \delta_H^*\left[1 - \left(\frac{u_\infty}{u_o H}\right)^2 (1 - Q)\right] \quad (102)$$

or, with the abbreviation,

$$\psi = \psi\left(k, \frac{u_o\ H}{u_\infty}\right) = \left(\frac{u_\infty}{u_o\ H}\right)^2 (1 - Q) - 1 \qquad (103)$$

finally:

$$W_d = \int_{I+II} \delta^* \frac{d\ p}{d\ s}\, dx - \psi\, \rho\, u_o^2\ H\ \delta_H^* \qquad (104)$$

Herewith the calculation of the pressure drag has been reduced to that of the displacement thickness δ^*, that is, to a friction layer quantity. According to figure 11, factor ψ is little dependent on the shape of the velocity profile at the trailing edge, but more on the ratio $\frac{u_o\ H}{u_\infty}$.

Addition of (77) and (104), with angle β disregarded, approximates the profile drag W_p of the wing to

$$W_p \sim \rho\, u_o^2\ H\ (2\, \vartheta_H - \psi\, \delta_H^*) \qquad (105)$$

Equation (105) permits particularly the reduction of the profile drag measurement in practice to a friction layer measurement on the trailing edge and therefore represents a welcome supplement to the Betz momentum method (reference 37).

But for purely theoretical solution of the total profile drag, equation (105) is still inapplicable for the present, because its principal constituent is the friction drag, and this will continue until the momentum thickness ϑ in the turbulent part of the friction layer can be determined without approximate assumptions on the shearing stress τ_o.

So, for the time being, the procedure of defining the profile drag will have to consist of computing τ_o as well as δ^* along the profile contour with the methods described in chapter III and then of the friction drag with (1) and the pressure drag with (104).

Before proceeding to the practical application of the proposed method, we wish to point out how the method may be employed to solve the real pressure distribution from a given potential pressure distribution, by iteration.

Starting from the potential pressure distribution, we compute with it the displacement thickness δ^*; the curve having the distance δ^* from the initial profile represents a new profile contour whose potential pressure distribution is obtained by transformation on the circle and presents a first approach to the actual pressure distribution of the initial profile. Then the displacement thickness δ^* for this pressure distribution is computed, affording a new profile contour, etc.

Now the developed method is being used to define the profile drag coefficient on the seven symmetrical Karman-Trefftz profiles studied by Fage, Falkner, and Walker (reference 35) in symmetrical flow.

V. APPLICATION TO THE SOLUTION OF PROFILE DRAG OF SEVEN SYMMETRICAL KARMAN-TREFFTZ PROFILES IN SYMMETRICAL FLOW

These profiles were chosen because their profile drag and pressure distribution was recorded at 6.58, 10.76, 15.32, 19.8, and 24.25 meters per second air speed; besides friction layer data for one were available (reference 32).

Thickness and trailing edge were so defined as to locate the maximum thickness at 1/3 wing chord. Then

$$\kappa = \frac{\overline{O_1 O_2}}{2a} \tag{106}$$

according to Glauert, but in Betz' method of identification (reference 16), where κ defines the trailing edge

$$\varphi = \kappa \cdot \pi \tag{107}$$

and

$$\epsilon = \frac{\overline{O_1 O_2}}{a} = 2\kappa \tag{108}$$

the thickness. The actual chord of the models in the tests was smaller by $\frac{0.2}{\epsilon}$ percent than the theoretical chord; the trailing edge was rounded off. The form parameters are given in table 1; the profiles themselves (fig. 12) are replicas of those in reference (35).

TABLE 1.- PROFILE PARAMETERS

Profile	ϵ	κ	φ (deg)	t_{theor} (m)	t_{actual} (m)	D_{max} (m)	d
1	0.0333	0.0167	3	1.462	1.375	0.0756	0.0551
2	.0667	.0333	6	1.51	1.465	.1524	.1040
3	.1	.05	9	1.03	1.009	.152	.1506
4	.1429	.0714	12.9	.7475	.736	.1524	.2069
5	.2	.1	18	.564	.559	.1524	.2726
6	.25	.125	22.5	.47	.466	.1524	.3270
7	.333	.1667	30	.373	.371	.1492	.4025

The kinematic viscosity of air is computed from the English data on Re, u_∞, and t, at $\nu = 1.48 \times 10^{-5}$ square meters per second.

From the pressure distributions plotted in figures 13 to 19, it is seen that, apart from profile 2, the distributions vary so little and with ascending Reynolds number so unsystematically from one another that the theoretical distribution, even on thick strut sections, may be looked upon as satisfactory up to 80 percent of the chord.

With the aid of the theoretical pressure distribution the laminar friction layer was computed for the lowest wind speed of $u_\infty = 6.58$ meters per second according to the Pohlhausen method. As direct graphical result of the isocline method, figure 20 shows the values of $\frac{Z}{t}\frac{u_\infty}{} = \left(\frac{\delta}{t}\right)^2 Re$ (see (31)) plotted against the arc length up to the value where the theory stipulates separation in laminar friction layer. In figure 21, the location of the separation point $\frac{x_a}{t}$ of the laminar layer is plotted against profile thickness d, along with the corresponding values for symmetrical Joukowski profiles according to Kosmodemiansky (reference 24) and the separation point for the circular cylinder (d = 1) by Hiemenz and the circular cylinder $\left(d = \frac{a_2}{a_1} = 0.338\right)$ by Schubauer.

From Z the Pohlhausen boundary layer thickness δ can be obtained with (31), so that the characteristic quantities of the laminar friction layer λ, δ^*, ϑ

and τ_o (figs. 22 to 24) can be computed from (26), (28), (29), and (30). The corresponding values of δ^*, ϑ, and τ_o for $u_\infty = 15.32$ meters per second and $u_\infty = 24.45$ meters per second wind speed, as afforded from (37) by conversion from the values for $u_\infty = 6.58$ meters per second are shown individually in figures 25 to 36.

For the selection of the transition points the Reynolds number $Re_\vartheta = \frac{u_o \vartheta}{\nu}$ was plotted against the arc length with speed u_∞ as parameter, and then several points chosen arbitrarily from Gruschwitz' quoted Re_ϑ = range.

Figures 25 to 36 illustrate the momentum thickness ϑ, the form parameter η, and the displacement thickness δ^* in the turbulent friction layer conformal to Gruschwitz' solution for profiles 1, 3, 5, and 7 and air speeds $u_\infty = 6.58$, 15.32, 24.45 meters per second at different transition point locations. Before the transition points are the values of the laminar friction layer obtained by Pohlhausen theory.

That ϑ and δ^* in the transition point are computed identically is due to the fact that the basic value $\eta = 0.1$ in the transition point defines a value of $H = \frac{\delta^*}{\vartheta} \sim 1$. It is known from experiment that the displacement thickness on the transition point frequently grows very rapidly almost discontinuous. Since the amount of this discontinuity cannot be computed, quite apart from the fact that the η values immediately behind the transition point are themselves uncertain, the curve of δ^* over a certain distance behind the transition point is not accurately determinable. For the calculation of the pressure drag the laminar displacement thickness was therefore continued with a somewhat arbitrary curve up to the more safely defined δ^* values in the rear portion of the profiles. These connecting curves are not shown.

As the characteristic quantities in the turbulent friction layer cannot be reduced from one $Re = \frac{u_\infty t}{\nu}$ to another, they must be graphically and numerically defined for each Reynolds number.

The momentum thickness ϑ in the turbulent layer is seen to grow so much more at constant wind speed as the separation occurs earlier. It is also apparent that the form parameter η at some distance from the transition point is not substantially affected by a displacement of the transition point nor by the Reynolds number. It may therefore be asserted that, in the range of Re considered here at least, the region of separation of the turbulent friction layer on the wing is itself not very profoundly affected by the Reynolds number (fig. 37), as suspected, in fact, by Lyon (reference 38); it is likewise apparent from the experimental pressure distributions whose departure from the theoretical pressure distribution afforded a first rough estimation of the location of the separation point.

Figure 37 further discloses the forward shift of the region of separation x_a with growing profile thickness.

An unusual fact is that the separation criteria of Gruschwitz (75) and Nikuradse (76) yield the separation point at the same place (fig. 38).

In figures 39 to 50 the values of the shearing stress $\frac{\tau_o}{\rho u_\infty^2}$ are shown for three wind speeds plotted against $\frac{x}{t}$ for laminar and turbulent friction layer. The values of the turbulent friction layer were throughout computed according to (64). To illustrate the manner in which the shearing stress diverges from that of the friction sheet it was also plotted for the same Reynolds number Re = $\frac{u_\infty \cdot t}{\nu}$. This estimation yields, on the whole, too low drag values.

The shearing stress distribution on profile 3 at u_∞ = 24.45 meters per second wind speed (fig. 48) reveals a good agreement of the theoretical values of τ_o with those obtained from the friction layer measurements (reference 32).

From the shearing stress curves, which at greater profile thickness must be modified so as to make this stress disappear in the separation point of the turbulent friction layer, the friction drag is obtained by iteration according to (1). Because the drag portions of

suction and pressure side are equal as a result of flow symmetry, the friction drag coefficient reads:

$$c_{w_r} = 4 \int_0^1 \frac{\tau_o}{\rho u_\infty^2} d\left(\frac{x}{t}\right) \qquad (109)$$

In figures 51 to 57 this coefficient c_{w_r} is shown plotted against the coordinate $\frac{x_u}{t}$ of the transition point for all seven profiles at varying wind speeds, along with the experimental friction drag factors of Fage, Falkner, and Walker after subtracting the pressure drag from the weighed total drag at $c_a = 0$. Since the transition point of these tests is not known, except for profile 3, its location was deduced conversely by plotting the experimental c_{w_r} value on the theoretical curve for $c_{w_r}\left(\frac{x_u}{t}\right)$. As the wind speed increases the transition point on all profiles moves forward, but without overstepping the pressure minimum. On profile 3 and at $u_\infty = 24.45$ meters per second the experimentally defined transition point is located at $x_u/t = 0.24$ compared with $\frac{x_u}{t} = 0.27$ for the experimental c_{w_r} value in figure 53. Figures 51 to 57 further contain the coefficients of the equivalent friction sheets according to Betz' and Jones' approximation (sec. II) where x_u/t is to be computed by (5). Comparison discloses that Betz' equation (7) already gives a very good replica of the friction drag for medium wing thickness.

The pressure drag coefficient follows from (104) at

$$c_{w_d} = -4 \int_0^1 \frac{\delta^*}{t} \frac{u_o}{u_\infty} \frac{d}{d\, s/t}\left(\frac{u_o}{u_\infty}\right) d\left(\frac{x}{t}\right) - 2\psi \left(\frac{u_o H}{u_\infty}\right)^2 \frac{\delta_H^*}{t} \qquad (110)$$

A careful study discloses that the pressure drag coefficient also drops by constant Reynolds number if the transition point is left to shift backward, although this relation is too insignificant to warrant graphical representation. Figure 58 shows the theoretical and experimental pressure drag plotted against profile thickness at three wind speeds; the agreement is satisfactory as long as the friction layer does not become separated. The consistently slightly lower theoretical pressure drag

values are likely to be due to the fact that the Gruschwitz solution yields unusually high moment and displacement thickness values toward the trailing edge, as has been pointed out. Figure 59 shows the change in pressure and friction drag by constant Reynolds number, as copied from reference (35).

In conclusion, it can be stated that with the available data on the flow in the friction layer, the profile drag can be approximately computed, provided the location of the transition point is accurately known.

VI. GENERAL CONCLUSIONS

As shown in section V, the location of the transition point is of decisive importance for the theoretical solution of the profile drag. Since the available data for a positive identification of this point are inadequate, the available experimental findings in conjunction with the results of the present calculation are employed in an attempt to find this point even if only very roughly.

The suspicion that the location of the transition point is related with the pressure distribution over the surface of the body suggests the study of relationship of Reynolds number $Re_\vartheta = \frac{u_o \vartheta}{\nu}$ in the transition point with the dimensionless quantity $\frac{\vartheta}{u_o}\frac{du_o}{ds}$ in the transition point. Gruschwitz (reference 26) labored on a solution of this problem but was unable to establish a relation between the two quantities. Fage (reference 30) also merely found that the Reynolds number $Re^*_{\delta^*} = \sqrt{\frac{\tau_o}{\rho}}\frac{\delta^*}{\nu}$ in the transition point is not very much dependent on the pressure distribution.

Therefore, assuming that the comparison of the experimental friction drag factors on the thin Karman-Trefftz profiles of Fage, Falkner, and Walker (reference 35) with our theoretically computed values, gives the location of the transition point conformal to figures 51 to 57 sufficiently accurate affords additional data for exploring the relation of Re_ϑ in the transition point and $\frac{\vartheta}{u_o}\frac{du_o}{ds}$ in the transition point. The satisfactory

accuracy of our calculation may be considered proved by the fact that on profile 3 the experimentally defined transition point (reference 32) lies at $x_u = 0.24\ t$ against our $x_u = 0.27\ t$.

Figure 60 illustrates how on profiles 1 to 6 at varying wind speed the dimensionless quantity $-\frac{\vartheta}{u_o}\frac{d\,u_o}{d\,s}$ changes with Re_ϑ over the profile contour, the intersection points of the curves with the Re_ϑ axis defining the pressure minima on the profile. Each curve shows the point in which, according to figures 51 to 57, the transition occurs. Also shown are the corresponding values in the transition points obtained by Gruschwitz and his test series IV, V and airfoil section no. 387 at $\alpha = 12°$, those by Stüper (reference 33) for his test series I to IV, and those by Fage and Falkner (reference 32) on profile no. 3.

It is evident that this multiplicity of points establishes no definite relationship between Re_ϑ and $\frac{\vartheta}{u_o}\frac{d\,u_o}{d\,s}$ in the transition point. But it is startling that the pressure gradient is apparently quite unimportant as far as transition is concerned and that the value of Re_ϑ is largely decisive. All the Re_ϑ values of the transition points are within Dryden's range of $210 < Re_\vartheta < 680$ (fig. 5). The reason the "street" of the Re_ϑ values is so wide may have its basis in the different degree of turbulence of the air stream and the different surface roughness. Small Re_ϑ values in the transition point signify high turbulence or considerable roughness, large Re_ϑ values, low turbulence and smooth surface.

If our presumption that the transition point is independent of the pressure gradient and merely affected by turbulence and roughness is correct, then the transition point must also be able to shift before the pressure minimum by constant turbulence and given roughness, when the Reynolds number $Re = \frac{u_\infty\, t}{\nu}$ is large enough. For, from (36) follows that

$$\frac{Re_{\vartheta_2}}{Re_{\vartheta_1}} = \sqrt{\frac{Re_2}{Re_1}} \qquad (111)$$

in a fixed profile point. From the test data available this fact has been scarcely recognized whence the general opinion that the transition point did not shift beyond the pressure minimum. The present analysis at any rate makes it plausible that the pressure minimum does not form such a boundary for the transition point and that the reason such a location could not be satisfactorily ascertained is solely due to the too low Reynolds numbers $Re = \frac{u_\infty t}{\nu}$ of the experimental material.

A test at $Re = 10^7$ made in the meantime appears to confirm this assumption. Gruschwitz' measurements ranged between $8.5 \times 10^5 < Re < 2.6 \times 10^6$, Stüper's between $2.8 \times 10^6 < Re < 4.9 \times 10^6$, and Fage, Falkner, and Walker's between $1.7 \times 10^5 < Re < 2.4 \times 10^6$.

Figure 61 shows Re_ϑ plotted against the arc length of profile 4 for five different Reynolds numbers. The lowest three curves represent the Fage, Falkner, and Walker test series at $u_\infty = 6.58$ meters per second, 15.32 meters per second, and 24.45 meters per second.

The transition points obtained with the criterion (50) $Re_\vartheta = 460$ are located behind the pressure minimum. But by a tenfold or a hundredfold increase of the lowest Re the criterion $Re_\vartheta = 460$ would bring the transition points before the pressure minimum.

In conclusion, our presumption that the transition point is simply characterized by a certain Re_ϑ value which itself is dependent upon turbulence and roughness is to be used to compute theoretically the behavior of the profile drag at much larger Reynolds numbers than ever reached in the test. Base the transition criterion by moderate turbulence on the condition of, say, $Re_\vartheta = 460$; then the transition point, and hence the turbulent friction layer, can be computed with the aid of the laminar momentum thickness. The calculation, involving the profiles 1 to 4, consists in ascertaining the two portions of the profile drag at Reynolds number exactly 1/10 or 2/10 percent larger than the lowest experimental Reynolds numbers Re_{min} used by Fage, Falkner, and Walker. Since at this divergent Reynolds number Gruschwitz' approximate assumption (59) for τ_0 can no longer be used to compute the turbulent friction layer, the new average values

$\frac{Re}{Re_{min}}$	1	10	100
$\frac{\tau_o}{\rho u_o^2}$	0.002	0.00175	0.00125

are computed according to equations (6) and (68).

It appears that at large Reynolds numbers the pressure drag coefficient drops but very little with increasing Re, while the friction drag coefficient continues to decrease uniformly. Because of it the percent portion of the pressure drag would rise considerably with ascending Re. This shift of the portion of friction and pressure drag with increasing Re would also favor the most appropriate shape of the wing to the extent that with ascending Re a decrease in pressure drag becomes increasingly more important, that is, more slender profiles would have to be used with increasing Reynolds number.

In order to be able to remove the uncertainties still afflicting the present calculations the principles of the theory require a still better explanation in some points; the most urgent problems are:

1. A more definite identification of the location of the transition point

2. A more reliable arithmetic method for solving the shearing stress in the turbulent friction layer

3. Clarification of the discrepancy between experimentally and theoretically defined momentum thickness in the turbulent friction layer near the trailing edge.

Not until these problems have been solved satisfactorily will it be possible to compute the profile drag of a wing in purely theoretical manner with the necessary accuracy.

The drag proportions for the four profiles then are:

$\frac{Re}{Re_{min}}$	1				10				100			
Profile	1	2	3	4	1	2	3	4	1	2	3	4
c_{w_r}	0.0052	0.0065	0.0082	0.0084	0.0066	0.0069	0.0077	0.0084	0.004	0.0044	0.005	0.0056
c_{w_d}	.0012	.0023	.0026	.0048	.0006	.0011	.0013	.0019	.0005	.0008	.0011	.0016
$c_{w_{tot}}$	.0064	.0088	.0108	.0132	.0072	.008	.009	.0103	.0045	.0052	.0061	.0072
$\frac{c_{w_d}}{c_{w_{tot}}}$	.188	.261	.241	.363	.083	.137	.144	.184	.111	.154	.180	.222

REFERENCES

1. Prandtl, L.: Abriss der Strömungslehre. F. Vieweg, (Braunschweig) 1935 (2nd ed.).

2. Prandtl, L.: The Mechanics of Viscous Fluids. Vol. III of Aerodynamic Theory, W. F. Durand, ed., Julius Springer (Berlin), 1935.

3. Prandtl, L., and Schlichting, H.: Das Widerstandsgesetz rauher Platten. Werft. Reederei Hafen, vol. 15, no. 1, Jan. 1934, pp. 1–4.

4. Jones, B. M.: Skin Friction and the Drag of Streamline Bodies. R. and M. No. 1199, British A.R.C., 1928.

5. Hoerner, S.: Berechnung des Oberflächenreibungswiderstandes schneller Flugzeuge. Luftfahrtforschung, Bd. 12, Nr. 6, Oct. 3, 1935, pp. 188–92.

6. Betz, A.: Untersuchung einer Schukowskyschen Tragfläche. Z.F.M., Jahrg. VI, Heft 23 and 24, Dec. 24, 1915, pp. 173–79.

7. Bock, G.: Wege zur Leistungssteigerung im Flugzeugbau. Luftwissen, Bd. 4, no. 4, pp. 104–15, April 1937.

8. Dryden, H. L., and Kuethe, A. M.: Effect of Turbulence in Wind Tunnel Measurements. Rep. 342, NACA, 1930.

9. Doetsch, H.: Profilwiderstandsmessungen im grossen Windkanal der DVL. Luftfahrtforschung, Bd. 14, Lfg. 4/5, April 20, 1937, pp. 173–78.

10. Doetsch, H., and Kramer, M.: Systematische Profiluntersuchungen im grossen Windkanal der DVL. Luftfahrtforschung, Bd. 14, Lfg. 10, Oct. 12, 1937, pp. 480–5.

11. Munk, M. M.: The Principles of Aerodynamics. New York, 1933, pp. 130–37.

12. Munk, M. M., and Hückel, E.: Der Profilwiderstand von Tragflügeln. Technische Berichte der Flugzeugmeisterei, Bd. 2, Heft 3.

13. Jacobs, Eastman N., Ward, Kenneth E., and Pinkerton, Robert M.: The Characteristics of 78 Related Airfoil Sections from Tests in the Variable-Density Wind Tunnel. Rep. 460, NACA, 1933.

14. Glass, Th.: Scale Effect and the Dependence of the Profile Drag on Aerofoil Geometrical Parameters. CAHI, no. 286, 1936. (Russian)

15. Hoerner, S.: Versuche mit Kugeln betreffend Kennzahl, Turbulenz, und Oberflächenbeschaffenheit. Luftfahrtforschung, Bd. 12, Nr. 1, March 28, 1935, pp. 42–54.

16. Betz, A., and Keune, F.: Verallgemeinerte Kármán–Trefftz–Profile. Luftfahrtforschung, Bd. 13, Nr. 9, Sept. 20, 1936, pp. 336–45.

17. Theodorsen, Theodore: Theory of Wing Sections of Arbitrary Sahpe. Rep. 411, NACA, 1931.

18. Theodorsen, T., and Garrick, I. E.: General Potential Theory of Arbitrary Wing Sections. Rep. 452, NACA, 1933.

19. Pinkerton, Robert M.: Calculated and Measured Pressure Distributions over the Midspan Section of the NACA 4412 Airfoil. Rep. 563, NACA, 1936.

20. Pohlhausen, K.: Zur naherungsweisen Integration der Differentialgleichung der laminaren Grenzschicht. Z.f.a.M.M., Bd. 1, Heft 4, Aug. 1921, pp. 252–68.

21. Howarth, L.: Steady Flow in the Boundary Layer near the Surface of a Cylinder in a Stream. R. and M. No. 1632, British A.R.C., 1934.

22. Tollmein, W.: Grenzschichttheorie. In Wien–Harms, Handbuch der Experimentalphysik IV, 1, 1931.

23. Schubauer, G. B.: Air Flow in a Separating Laminar Boundary Layer. Rep. 527, NACA, 1935.

24. Kosmodemiansky, A.: Contribution to the Drag Theory. CAHI, no. 215, 1935. (Russian)

25. Golubew, W. W.: Investigations into the Theory of Slotted Aeroplane Wing. CAHI, no. 147, 1933. (Russian)

26. Gruschwitz, E.: Die turbulente Reibungsschicht in ebener Stromung bei Druckabfall und Druckanstieg. Ingenieur–Archiv, vol. 2, no. 3, Sept. 1931, pp. 321–46.

27. Schmidbauer, Hans: Behavior of Turbulent Boundary Layers on Curved Convex Walls. T.M. No. 791, NACA, 1936.

28. Peters, H.: On the Separation of Turbulent Boundary Layers. Jour. Aero. Sci., vol. 3, no. 1, Sept. 1935, pp. 7–12.

29. Dryden, Hugh L.: Air Flow in the Boundary Layer near a Plate. Rep. No. 562, NACA, 1936.

30. Fage, A.: On Reynolds Numbers of Transition. R. and M. No. 1765, British A.R.C., 1937.

31. Nikuradse, J.: Untersuchungen über die Strömungen des Wassers in konvergenten und divergenten Kanalen. Forschungsarbeiten auf dem Gebiete des Ingenieurwesens, no. 289, 1929.

32. Fage, A., and Falkner, V. M.: An Experimental Determination of the Intensity of Friction on the Surface of an Aerofoil. R. and M. No. 1315, British A.R.C., 1931.

33. Stüper, J.: Investigation of Boundary Layers on an Airplane Wing in Free Flight. T.M. No. 751, NACA, 1934.

34. Amtsberg, H.: Untersuchungen über die Formabhängigkeit des Reibungswiderstandes. Mitt. d. Preuss. Versuchsanst. f. Wasserbau und Schiffbau (Berlin), Heft 28, 1937.

35. Fage, A., Falkner, V. M., and Walker, W. S.: Experiments on a Series of Symmetrical Joukowski Sections R. and M. No. 1241, British A.R.C., 1929.

36. Betz, A.: Aufgaben und Aussichten der Theorie in der Strömungsforschung. Lilienthalgesellschaft für Luftfahrtforschung Jahrbuch 1936, pp. 21–28.

37. Betz, A.: A Method for the Direct Determination of Wing-Section Drag. T.M. No. 337, NACA, 1925.

38. Lyon, H. M.: Boundary Layer Theory. Aircraft Eng., vol. VII, no. 72, Feb. 1935, pp. 32–36.

Translation by J. Vanier,
National Advisory Committee
for Aeronautics.

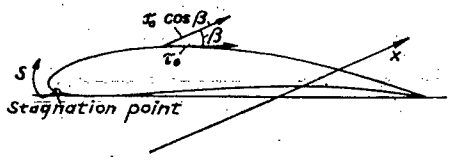

Figure 1.-Definition of friction drag.

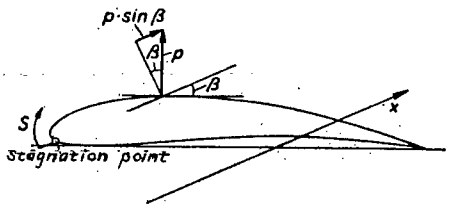

Figure 2.-Definition of pressure drag.

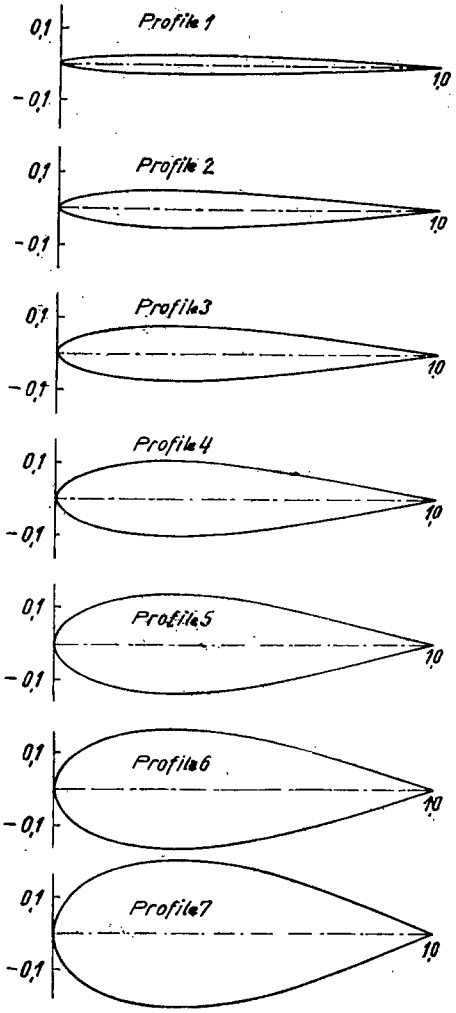

Figure 12.-Seven symmetrical Karman-Trefftz profiles.

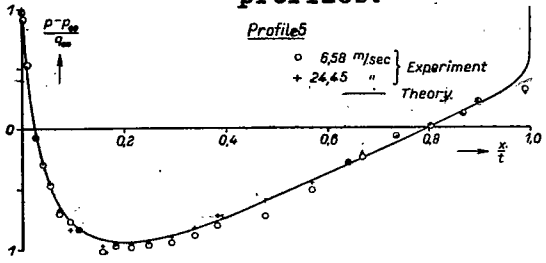

Figure 17.-Pressure distributions

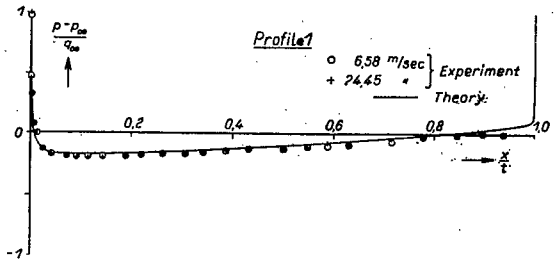

Figure 13.-Pressure distributions.

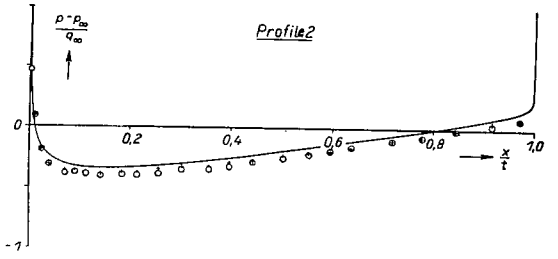

Figure 14.-Pressure distributions.

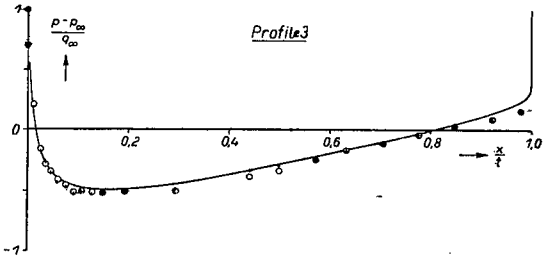

Figure 15.-Pressure distributions.

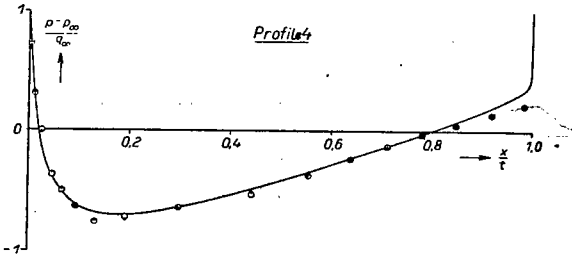

Figure 16.-Pressure distributions.

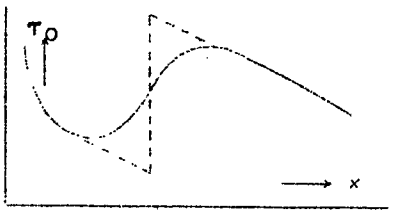

Transition point

Figure 3.-Effect of shearing stress in proximity of the transition point.

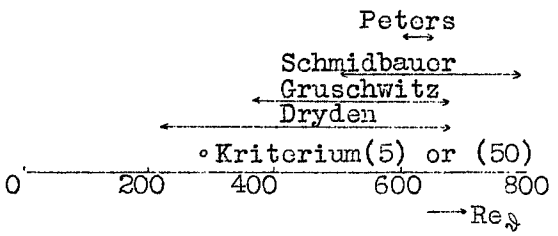

Figure 5.-Transition criteria.

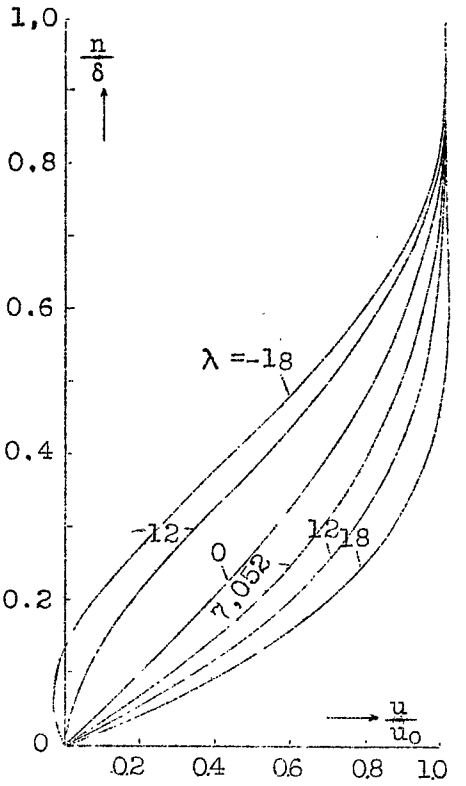

Figure 4.-Velocity profiles in laminar friction layer (according to Pohlhausen)

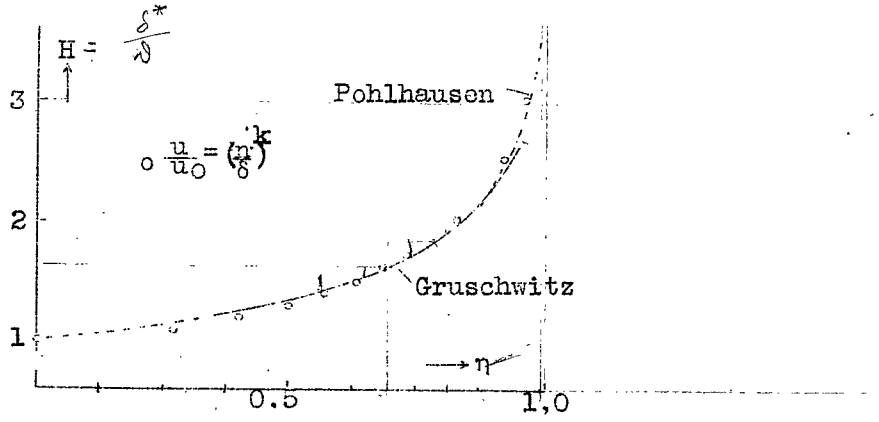

Figure 6.-Relation between form parameter η and quantity $H = \frac{\delta^*}{\vartheta}$ on turbulent velocity profiles.

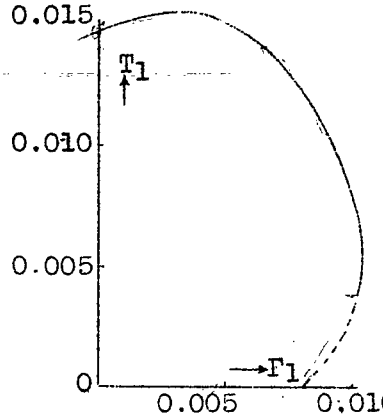

Figure 7.-Relation between $\Gamma_1 = -\frac{\delta^*}{u_o}\frac{du_o}{ds}\left(\frac{u_o\delta^*}{\nu}\right)^{\frac{1}{4}}$ and $T_1 = \frac{\tau_o}{\rho u_o^2}\left(\frac{u_o\delta^*}{\nu}\right)^{\frac{1}{4}}$ according to Nikuradse

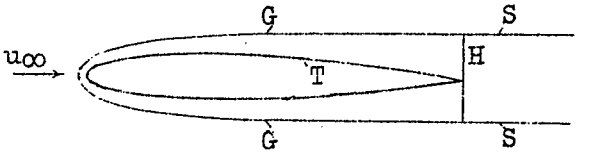

Figure 8.-Pressure drag.

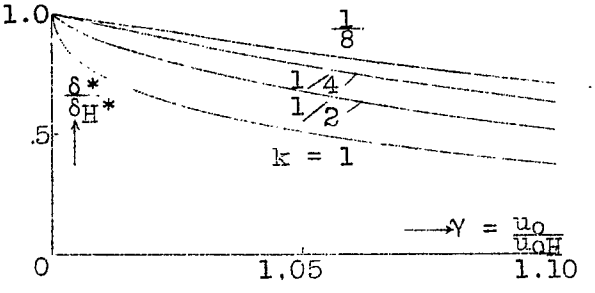

Figure 9.-Width of wake body.

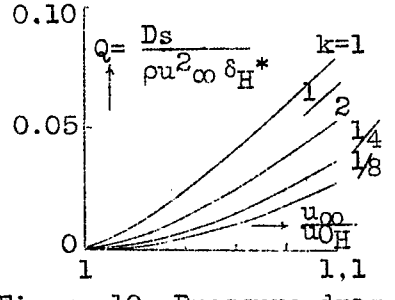

Figure 10.-Pressure drag coefficient of wake body $Q = \frac{D_s}{\rho u^2_\infty \delta_H^*}$

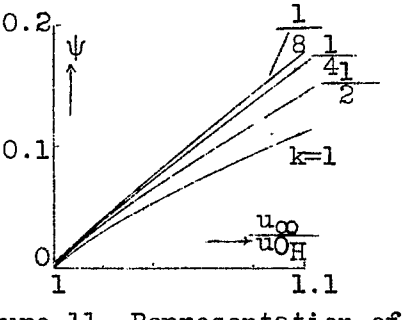

Figure 11.-Representation of factor ψ. (cf.eq. 103)

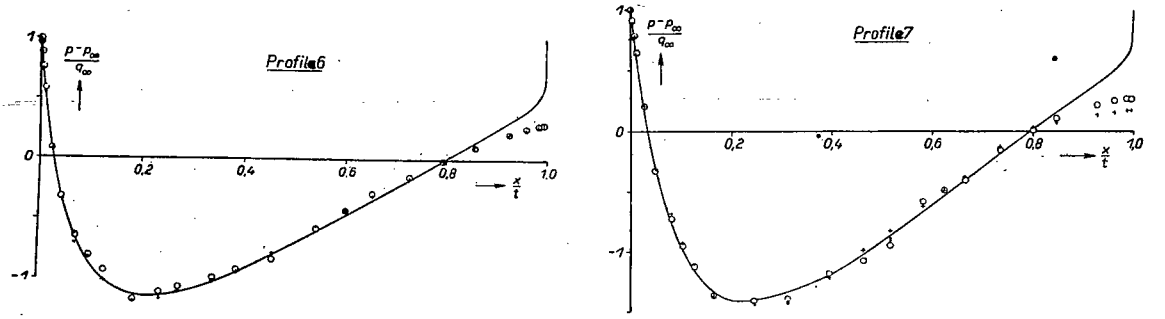

Figure 18-19.-Pressure distributions.

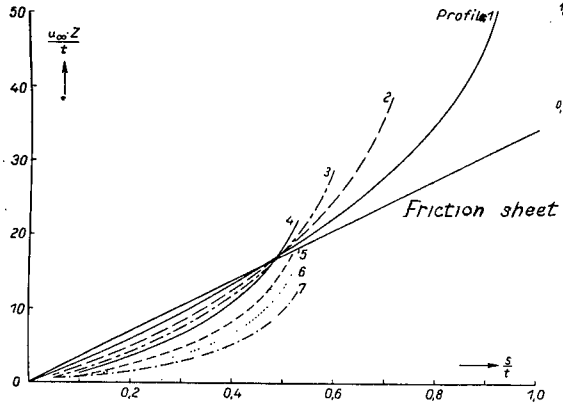

Figure 20.-Graphical result of Pohlhausen isocline method.

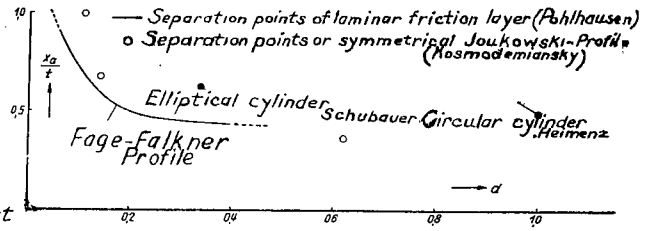

Figure 21.-Location of separation point of laminar layer plotted against profile thickness.

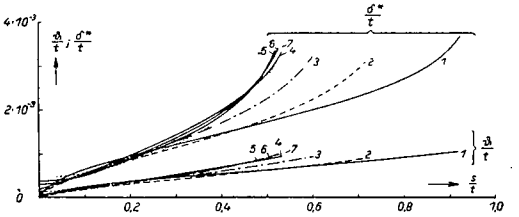

Figure 23.-Displacement thickness δ* and momentum thickness ϑ in laminar friction layer.

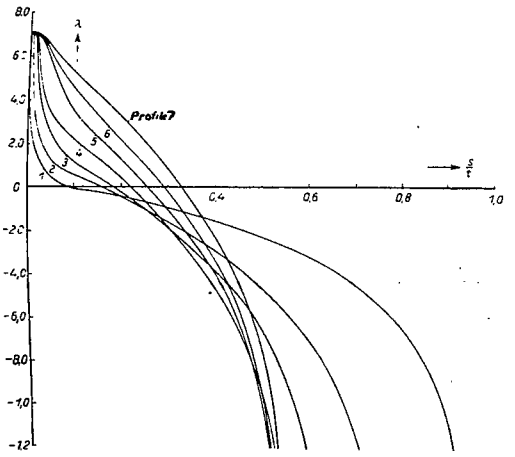

Figure 22.-Laminar form parameter λ.

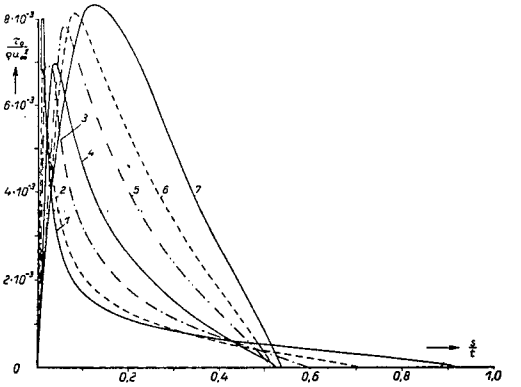

Figure 24.-Shearing stress τ_0 in laminar friction layer.

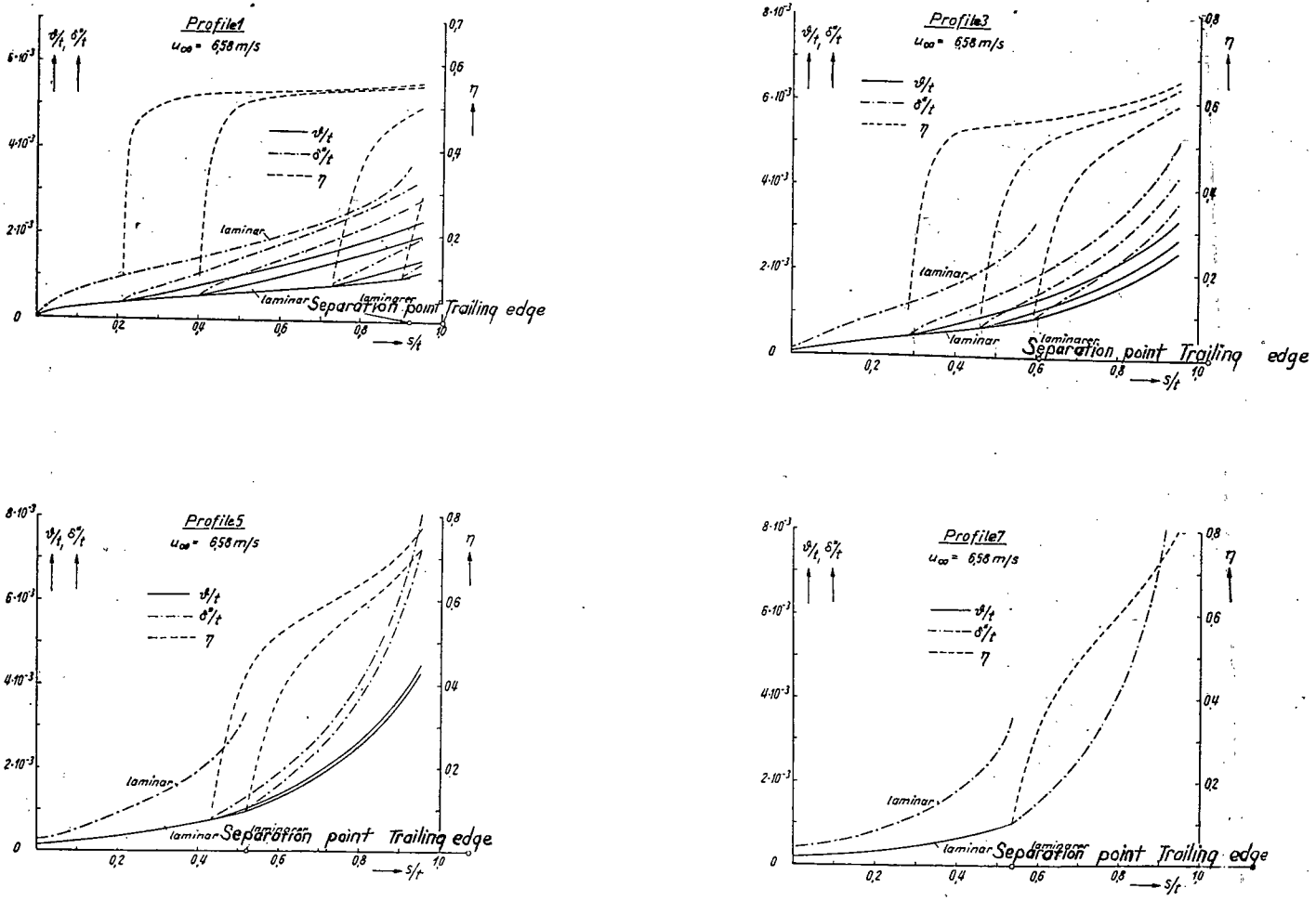

Figure 25-28.-δ^*, ϑ and η in laminar and turbulent friction layer for profile 1,3,5 and 7 at u_∞ = 6.58 m/s.

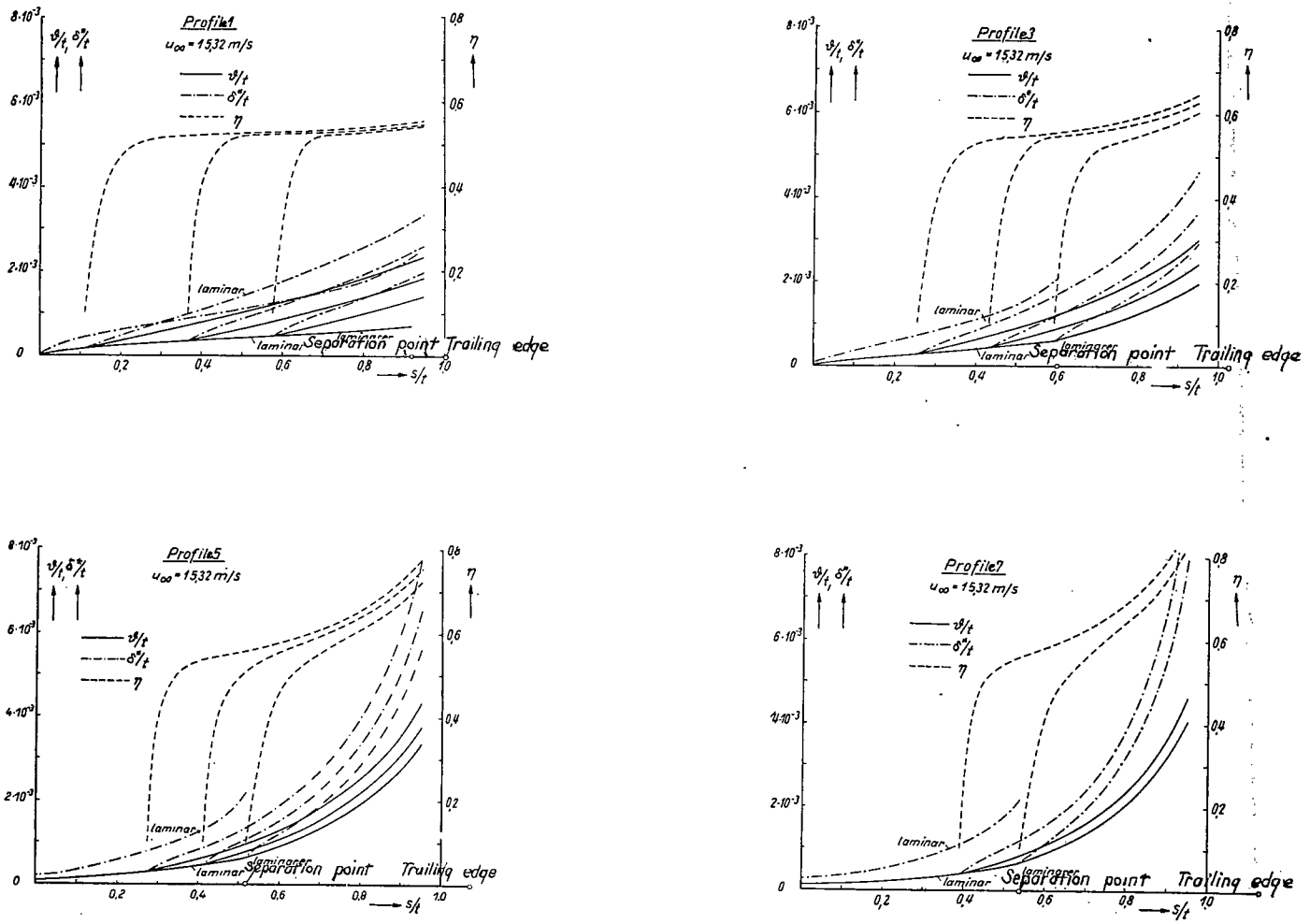

Figure 29-32.-δ^*, ϑ and η in laminar and turbulent friction layer for profile 1,3,5 and 7 at u_∞ = 15,32 m/s.

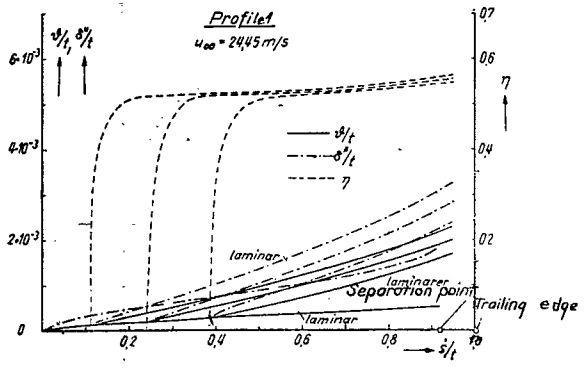

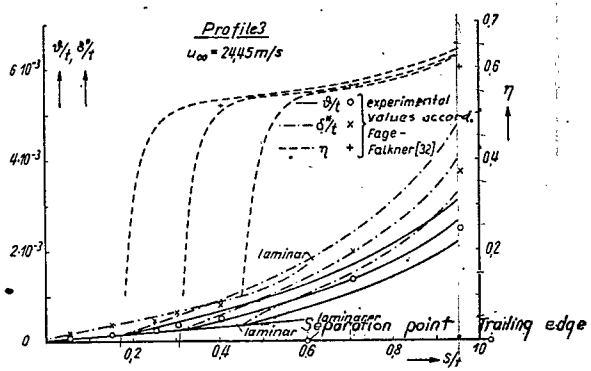

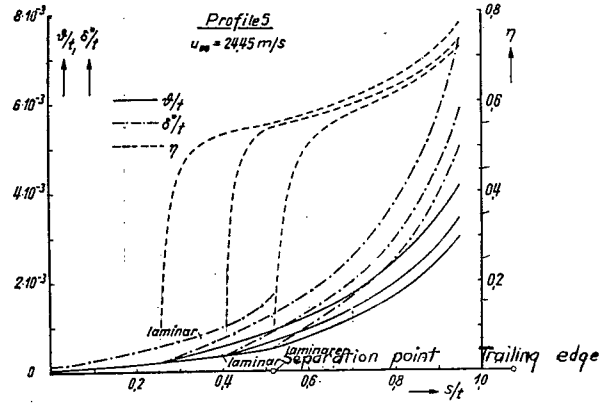

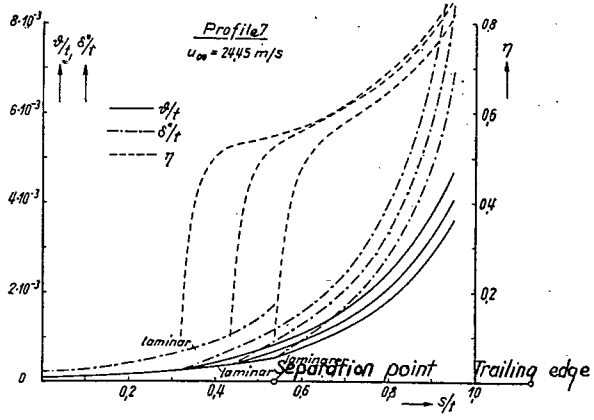

Figure 33-36.-δ^*,ϑ and η in laminar and turbulent friction layer for profile 1,3,5 and 7 at u_∞ = 24.45 m/s.

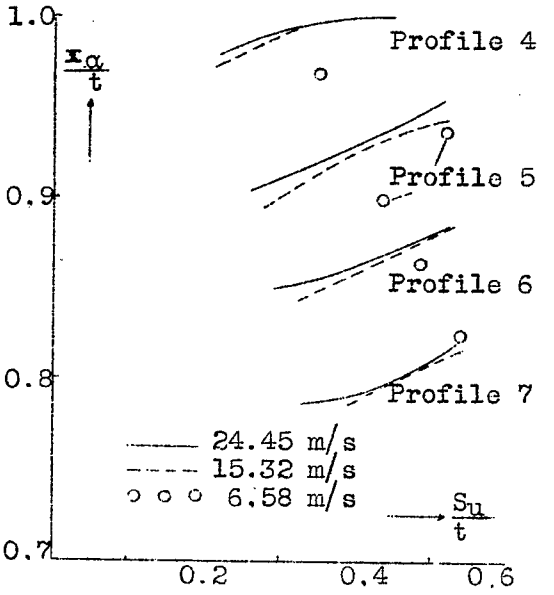

Figure 37.-Effect of choice of transition point on computed separation point of turbulent friction layer.

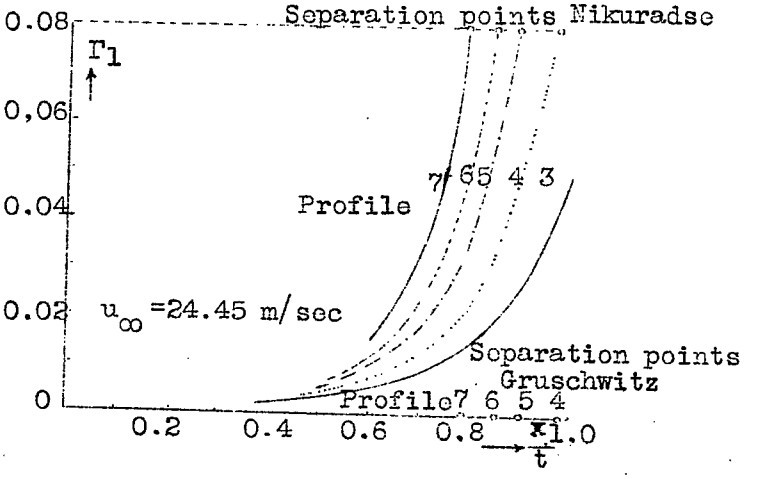

Figure 38.-Gruschwitz and Nikuradse separation points in turbulent friction layer.

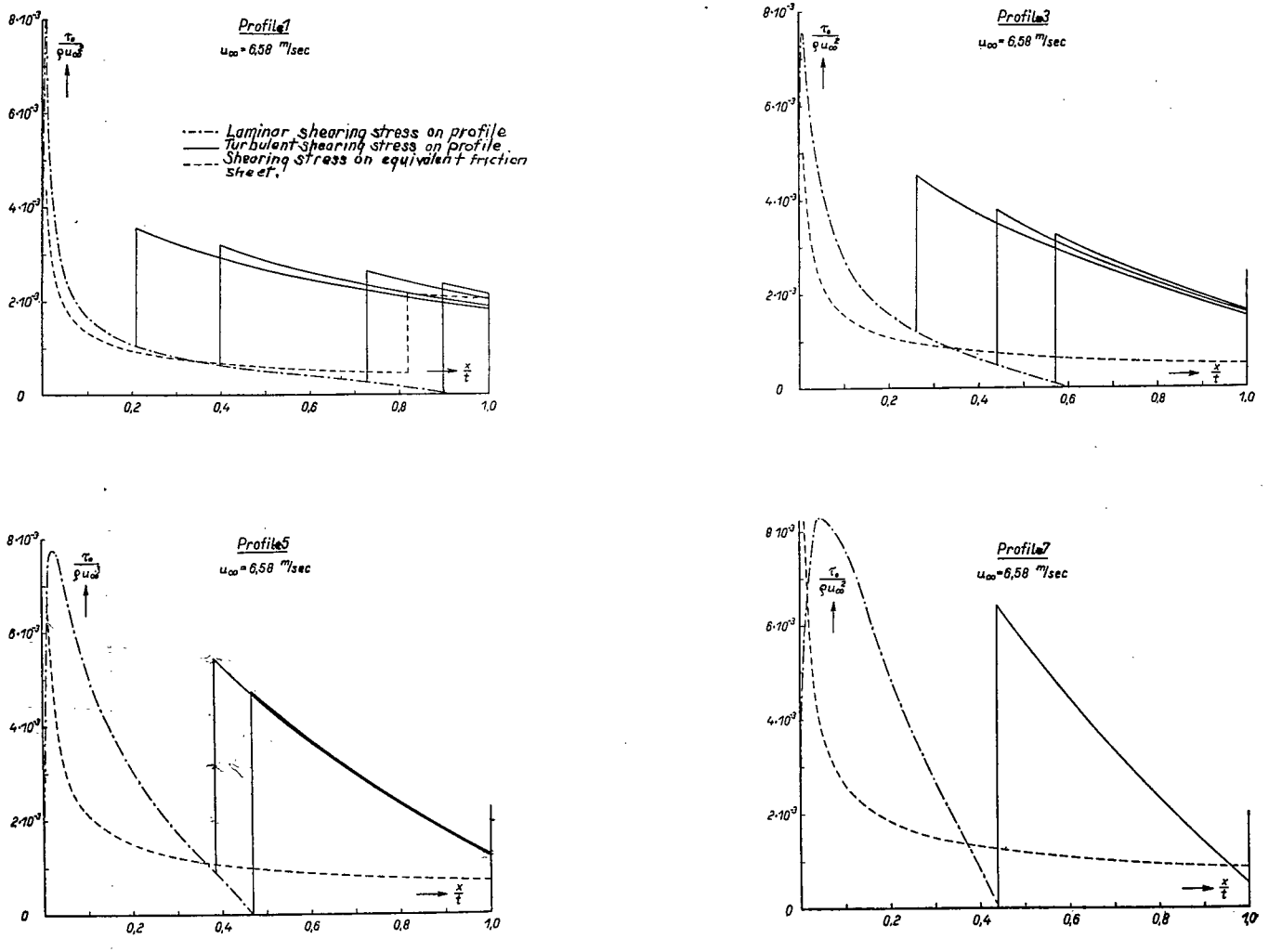

Figure 39-42.-Shearing stress τ_o in laminar and turbulent friction layer for profile 1,3,5 and 7 at u_∞ = 6.58 m/s.

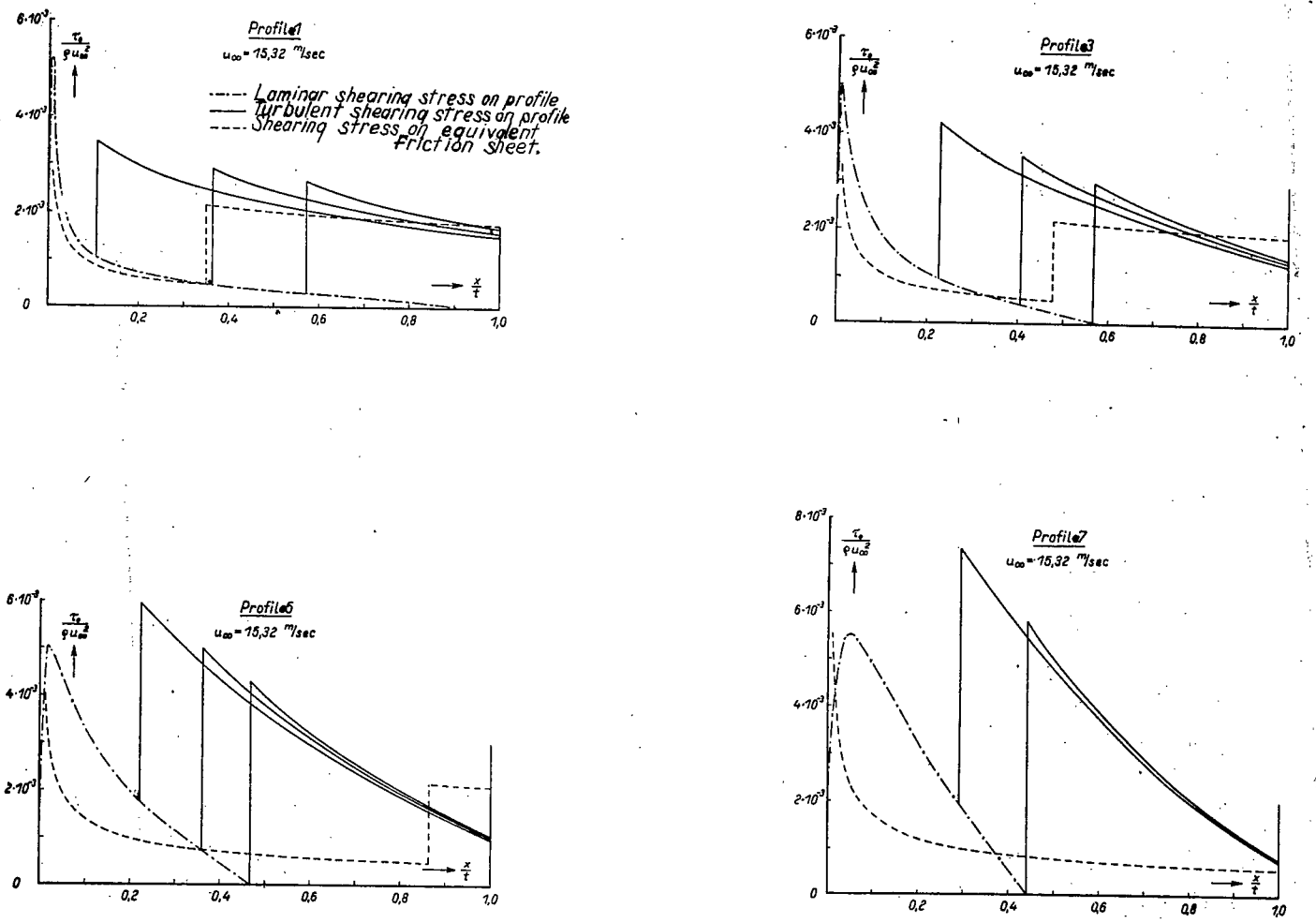

Figure 43-46.-Shearing stress τ_o in laminar and turbulent friction layer for profile 1,3,5, and 7 at u_∞ = 15.32 m/s.

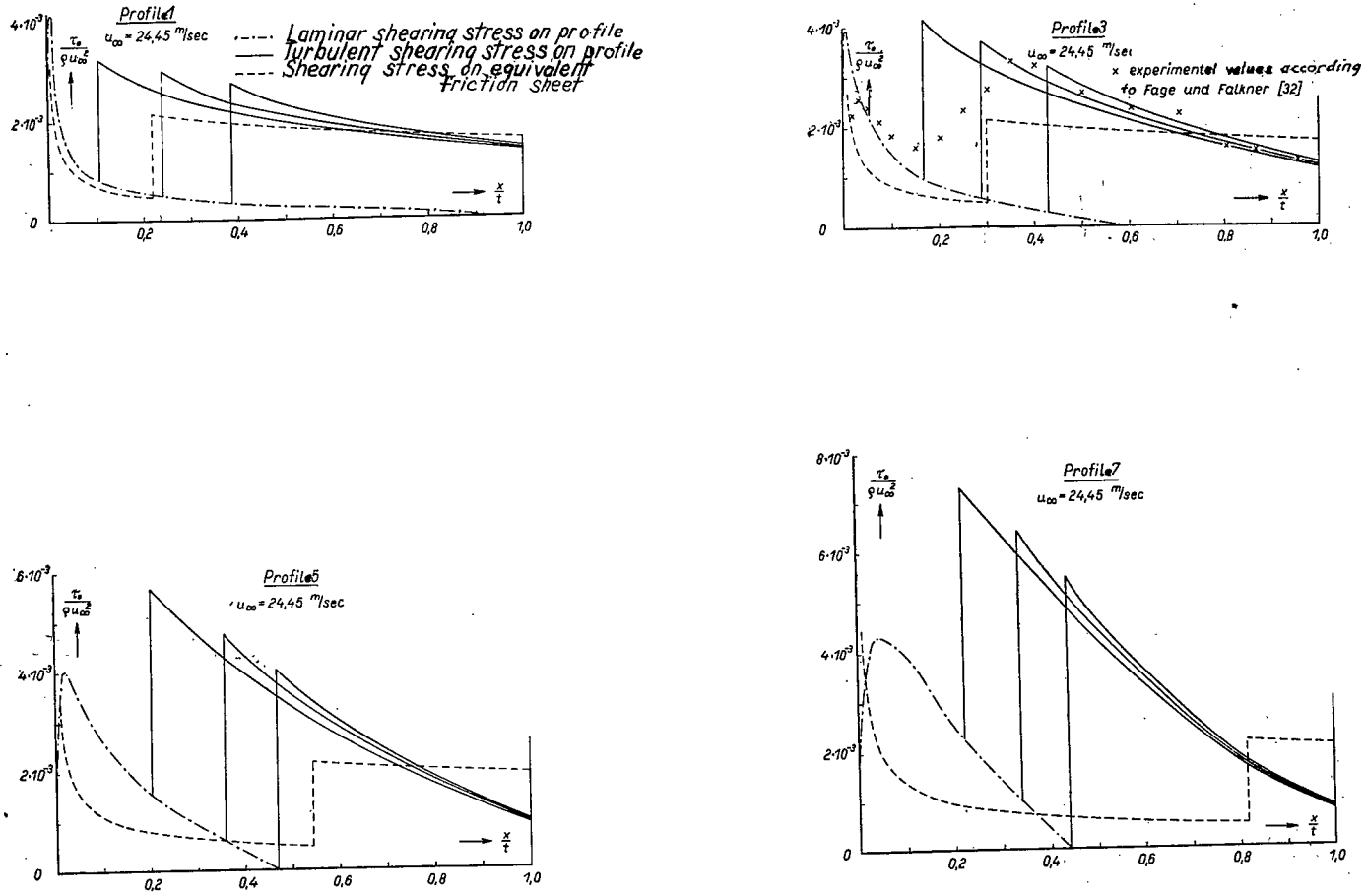

Figure 47-50.-Shearing stress τ_o in laminar and turbulent friction layer for profile 1,3,5 and 7 at u_∞ = 24.45 m/s.

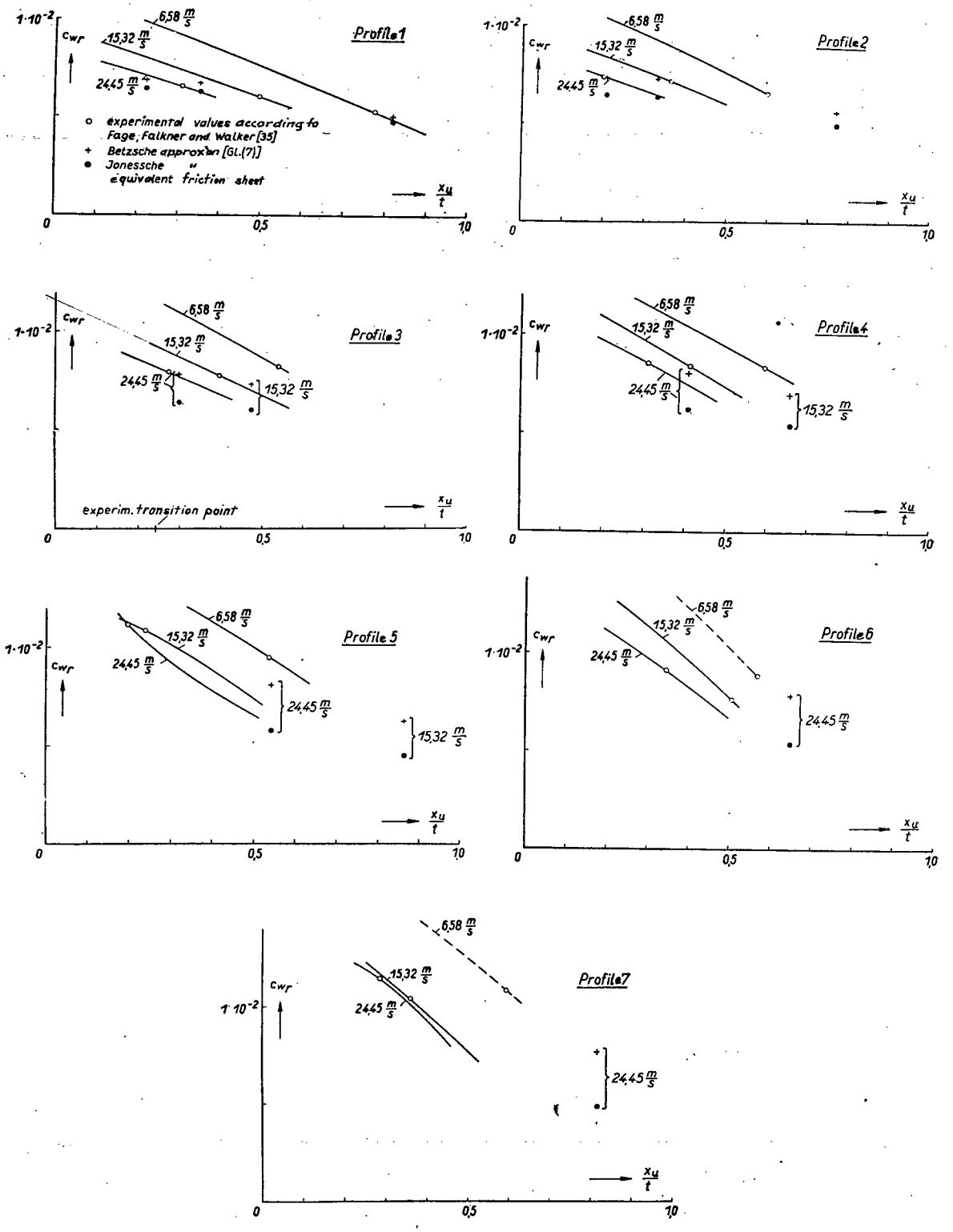

Figure 51-57.-Friction drag coefficient c_{wr} plotted against choice of transition point.

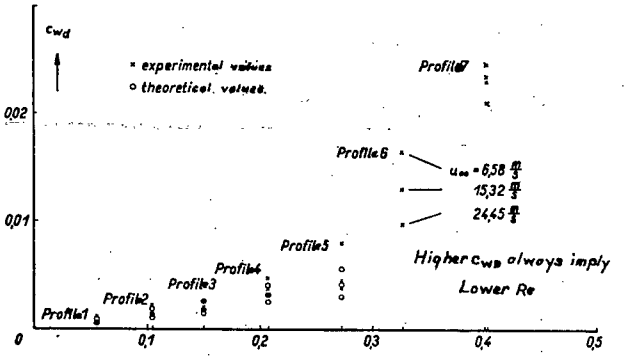

Figure 58.-Pressure drag coefficient c_{wd} plotted against profile thickness.

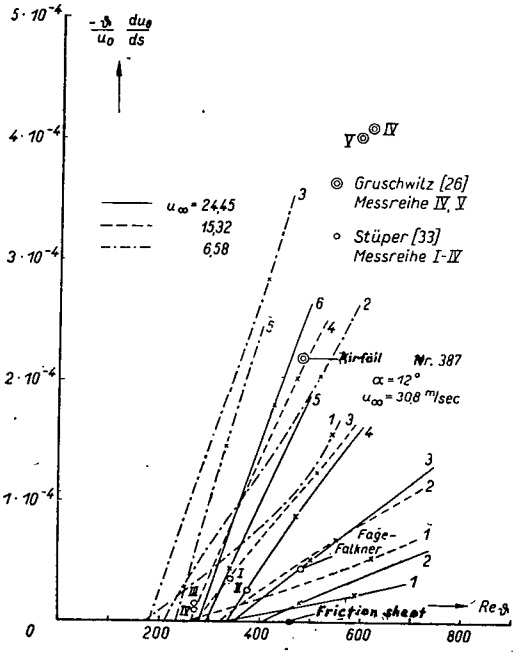

Figure 60.-Indentification of position of transitional point.

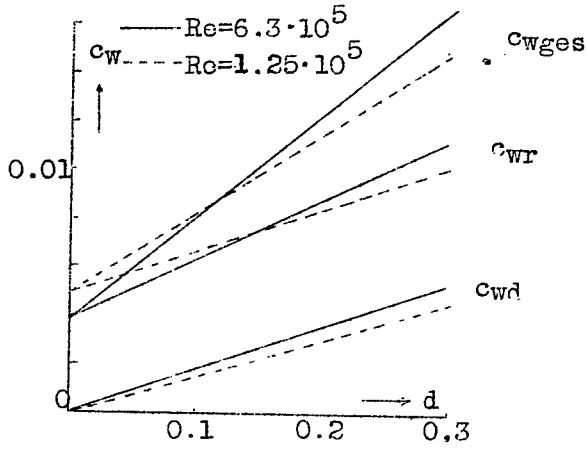

Figure 59.-Profile drag coefficient c_{wp} plotted against thickness at two Re.

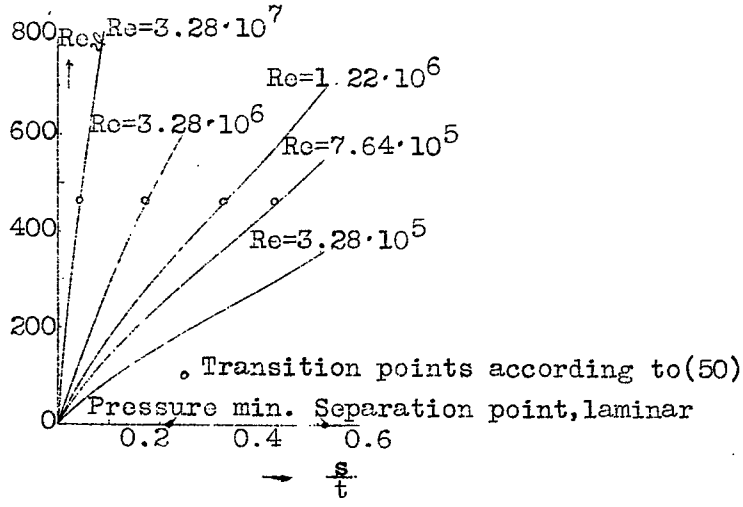

Figure 61.-Reynolds number Re_s plotted against the arc length on profile 4 at different Re.